Effects of inserting fluorescent proteins into the α_{1S} II–III loop: insights into excitation–contraction coupling

Roger A. Bannister,[1] Symeon Papadopoulos,[2] Claudia S. Haarmann,[2] and Kurt G. Beam[1]

[1]Department of Physiology and Biophysics, School of Medicine, University of Colorado Denver, Aurora, CO 80045
[2]Department of Biomedical Sciences, Neurosciences Division, Colorado State University, Fort Collins, CO 80523

In skeletal muscle, intermolecular communication between the 1,4-dihydropyridine receptor (DHPR) and RYR1 is bidirectional: orthograde coupling (skeletal excitation–contraction coupling) is observed as depolarization-induced Ca^{2+} release via RYR1, and retrograde coupling is manifested by increased L-type Ca^{2+} current via DHPR. A critical domain (residues 720–765) of the DHPR α_{1S} II–III loop plays an important but poorly understood role in bidirectional coupling with RYR1. In this study, we examine the consequences of fluorescent protein insertion into different positions within the α_{1S} II–III loop. In four constructs, a cyan fluorescent protein (CFP)–yellow fluorescent protein (YFP) tandem was introduced in place of residues 672–685 (the peptide A region). All four constructs supported efficient bidirectional coupling as determined by the measurement of L-type current and myoplasmic Ca^{2+} transients. In contrast, insertion of a CFP–YFP tandem within the N-terminal portion of the critical domain (between residues 726 and 727) abolished bidirectional signaling. Bidirectional coupling was partially preserved when only a single YFP was inserted between residues 726 and 727. However, insertion of YFP near the C-terminal boundary of the critical domain (between residues 760 and 761) or in the conserved C-terminal portion of the α_{1S} II–III loop (between residues 785 and 786) eliminated bidirectional coupling. None of the fluorescent protein insertions, even those that interfered with signaling, significantly altered membrane expression or targeting. Thus, bidirectional signaling is ablated by insertions at two different sites in the C-terminal portion of the α_{1S} II–III loop. Significantly, our results indicate that the conserved portion of the α_{1S} II–III loop C terminal to the critical domain plays an important role in bidirectional coupling either by conveying conformational changes to the critical domain from other regions of the DHPR or by serving as a site of interaction with other junctional proteins such as RYR1.

The Journal of General Physiology

INTRODUCTION

The skeletal muscle L-type Ca^{2+} channel (1,4-dihydropyridine receptor [DHPR]) serves as the voltage sensor for excitation–contraction (EC) coupling (Tanabe et al., 1988), activating Ca^{2+} release from the SR via RYR1 in response to depolarization of the plasma membrane. The interaction with RYR1 also increases the magnitude of the L-type Ca^{2+} current produced by DHPR (Nakai et al., 1996; Grabner et al., 1999; Avila and Dirksen, 2000; Avila et al., 2001; Ahern et al., 2003; Sheridan et al., 2006). Neither of these interactions depends on any obvious diffusible messenger (such as entry of external Ca^{2+}), which has led to the idea that there is bidirectional conformational coupling between these two proteins (Tanabe et al., 1988; García and Beam, 1994; García et al., 1994; Nakai et al., 1998b; Grabner et al., 1999). Moreover, freeze-fracture replicas of the plasma membrane at sites of junction with the SR reveal a structural correlate of the functional interaction between DHPR and RYR1 (Block et al., 1988; Takekura et al., 1994, 2004; Protasi et al., 2002; Sheridan et al., 2006). Specifically, intramembranous particles in the plasma membrane, which appear to represent DHPRs, are arranged into groups of four (tetrads) with spacing that places them in register with the four subunits of every other RYR1. Moreover, the distance between each DHPR within the tetrad (~19 nm) is decreased (~2 nm) by application of a high concentration of ryanodine (Paolini et al., 2004), which locks RYR1 in an inactivated, nonconducting state (Buck et al., 1992; Zimányi et al., 1992). Thus, it seems quite certain that protein–protein interactions link DHPR and RYR1.

Two basic strategies have been used in the search to identify the protein–protein interactions that may couple the DHPR and RYR1. One approach has been biochemical analysis of isolated proteins. With this approach, it has been shown that specific regions of the DHPR bind to, or affect the function of, RYR1 and that specific regions of RYR1 bind to DHPR. This approach has revealed that segments of the α_{1S} II–III loop (Leong and

Correspondence to Kurt G. Beam: kurt.beam@ucdenver.edu

S. Papadopoulos' present address is Dept. of Physiology, Hannover Medical School, 30625 Hannover, Germany.

C.S. Haarmann's present address is Nanion Technologies GmbH, 80335 Munich, Germany.

Abbreviations used in this paper: CFP, cyan fluorescent protein; DHPR, 1,4-dihydropyridine receptor; EC, excitation–contraction; YFP, yellow fluorescent protein.

The Rockefeller University Press $30.00
J. Gen. Physiol. Vol. 134 No. 1 35–51
www.jgp.org/cgi/doi/10.1085/jgp.200910241

MacLennan, 1998a), α_{1S} III–IV loop (Leong and MacLennan, 1998b), and the proximal α_{1S} C terminus (Sencer et al., 2001) bind to fragments of RYR1 and that segments of RYR1 bind to DHPR subunits (Sencer et al., 2001; Cheng et al., 2005). An important limitation of such biochemical approaches is that they may reveal interactions between segments of proteins that do not interact within living cells. Moreover, the interactions revealed by these biochemical approaches have often been difficult to reconcile with results obtained by functional analyses of myotubes after expression of cDNAs encoding wild-type or engineered DHPRs or RYRs (Beam and Horowicz, 2004). For the functional analysis of the DHPR, the focus has been on the α_{1S} and β_{1a} subunits because bidirectional signaling is little affected by knockout/knockdown of the γ_1 (Freise et al., 2000; Ursu et al., 2001) or $\alpha_2\delta$-1 (Obermair et al., 2005, 2008; García et al., 2007; Gach et al., 2008; Tuluc et al., 2009) subunits. Expression of cDNAs in myotubes null for endogenous β_1 has revealed that the C terminus of β_{1a} is important for EC coupling (Beurg et al., 1999; Sheridan et al., 2003a,b, 2004). Likewise, expression of cDNAs in dysgenic (α_{1S} null) myotubes has shown that EC coupling is critically dependent on the α_{1S} II–III loop (see next paragraph) and is also influenced by the α_{1S} III–IV loop (Weiss et al., 2004; Bannister et al., 2008b).

The α_{1S} II–III loop substituted into the corresponding region of the cardiac DHPR α_{1C} subunit confers skeletal-type coupling (Tanabe et al., 1990; Carbonneau et al., 2005), and, conversely, substitution into an α_{1S} backbone with the II–III loop of α_{1C} (SkLC; Grabner et al., 1999) or α_{1M} (SkLM; Wilkens et al., 2001; Kugler et al., 2004b) abolishes bidirectional signaling. However, bidirectional signaling is restored when a critical domain of the α_{1S} II–III loop (residues 720–765; Nakai et al., 1998b) is reintroduced within SkLC or SkLM (Grabner et al., 1999; Wilkens et al., 2001; Kugler et al., 2004b). Within the critical domain, a central region (α_{1S} residues 737–751) contains the binding site (residues 737–744) for mAb 1A (Kugler et al., 2004a) and an adjacent cluster of negative charges (residues 744–751). Within this central region, mutation of Ala^{739}, Phe^{741}, Pro^{742}, or Asp^{744} to its corresponding α_{1C} residue reduces both skeletal-type EC coupling and the binding of mAb 1A, and the secondary structure of residues 744–751 also appears to be important for skeletal-type EC coupling (Kugler et al., 2004a,b). On the basis of these results, it has been proposed that some portion of α_{1S} residues 737–751 may bind to and activate RYR1 in response to conformational changes of other regions of the DHPR (Kugler et al., 2004b).

If conformationally driven interactions between regions of the α_{1S} II–III loop and RYR1 are important for bidirectional signaling, it is important to understand how those interactions are coupled to other regions of the DHPR. Previous work (Ahern et al., 2001b) has shown that skeletal-type EC coupling is preserved after expression of a one-piece α_{1S} construct lacking residues 671–690 (the peptide As-20 region; El-Hayek and Ikemoto, 1998). Moreover, two-fragment α_{1S} constructs created by deletion of residues 671–690 (Flucher et al., 2002) or 671–700 (Ahern et al., 2001a) also supported robust EC coupling. Although these results indicate that coupling does not require the presence of the peptide A region or the connection of the critical domain to α_{1S} repeat II via the peptide backbone, they do not exclude a modulatory role for this segment of the α_{1S} II–III loop, which has been recently reported to bind in vitro to a fragment of RYR1 (residues 1,085–1,208; Cui et al., 2009; Tae et al., 2009).

It is important to note that the α_{1S} II–III loop region extending from within the C-terminal portion of the critical domain to α_{1S} repeat III has not been adequately tested because this region of the loop is overall considerably conserved between α_{1S} and the corresponding regions of α_{1C} and α_{1M} (Wilkens et al., 2001). To examine more systematically the importance of different portions of the α_{1S} II–III loop, we introduced perturbations at distinct sites within the loop. In particular, we introduced substantial extra mass (one or two fluorescent proteins) at various sites. The rationale for this approach is that one would expect that sites able to accommodate this insertion without affecting function could neither directly interact with other junctional proteins nor undergo large conformational changes during EC coupling.

We have found that bidirectional coupling is not affected by insertion of a tandem of fluorescent proteins (aggregate mass of ~56 kD) in place of α_{1S} residues 672–685, adding support to the prevailing view that regions of the α_{1S} II–III loop flanking this insertion site do not undergo important conformational changes and that the critical domain does not interact with more proximal portions of the loop. We found that insertions located more toward the C-terminal end of the loop had a much larger impact on bidirectional signaling. Thus, bidirectional coupling was totally abolished by insertion of the tandem within the critical domain's N-terminal boundary (between α_{1S} residues 726 and 727) but only partially ablated by insertion of a single fluorescent protein at this site. However, bidirectional signaling was essentially ablated by the insertion of a single yellow fluorescent protein (YFP) near the C-terminal boundary of the critical domain (between α_{1S} residues 760 and 761). This also occurred when a single YFP was inserted between α_{1S} residues 785 and 786, which is C terminal to the critical domain and well conserved between α_{1S}, α_{1C}, and α_{1M}. Control experiments indicated that these insertions did not interfere with membrane expression or targeting to peripheral junctions. Thus, our results raise the possibility that the signaling functions of the critical domain depend on its linkage to α_{1S} repeat III via the C-terminal portion of the α_{1S} II–III loop. Alternatively, this conserved region of the α_{1S} II–III loop may be an important site of protein–protein interaction required for signaling.

MATERIALS AND METHODS

Molecular biology

The constructions of YFP-α_{1S}, α_{1S}(671-CFP-YFP-686), and α_{1S}(671-CFP-YFP) + (686)α_{1S} were previously described in Papadopoulos et al. (2004). All residue numbers refer to the amino sequence of rabbit α_{1S} (GenBank/EMBL/DDBJ accession no. X05921).

α_{1S}(671-CFP) and (YFP-686)α_{1S}. α_{1S}(671-CFP) and (YFP-686)α_{1S} encode, respectively, (a) α_{1S} residues 1–671 followed by an 11-residue linker and by cyan fluorescent protein (CFP) and (b) YFP followed by a 12-residue linker and by α_{1S} residues 686–1,860. To make α_{1S}(671-CFP), the sequence encoding α_{1S} 1–671 (2,039 bp) was excised from α_{1S}(671-CFP-YFP) with HindIII and KpnI and ligated into the polylinker of the mammalian expression vector pECFP-N1 (Clontech Laboratories, Inc.) cleaved by HindIII and KpnI (4,706-bp fragment). To make (YFP-686)α_{1S}, the sequence encompassing the region encoding YFP (769 bp) was excised from pEYFP-C1 (Clontech Laboratories, Inc.), which had been modified to bring the HindIII site into frame for the subsequent cloning procedure. Specifically, an XhoI–SalI fragment of the pEYFP-N1 polylinker encompassing the HindIII site was reversed by ligation into the compatible NheI and HindIII, which are sites of (686)α_{1S} (Papadopoulos et al., 2004) opened by NheI and HindIII (7,843 bp).

α_{1S}(671) and (CFP-YFP-686)α_{1S}. α_{1S}(671) and (CFP-YFP-686)α_{1S} encode, respectively, (a) α_{1S} residues 1–671 followed by a 12-residue linker and (b) the CFP–YFP tandem (separated by a 23-residue linker) followed by a 12-residue linker and by α_{1S} residues 686–1,860. To make untagged α_{1S}(671), the sequence encoding α_{1S}(671) (2,039 bp) was removed from α_{1S}(671-CFP) (see previous paragraph) with HindIII and KpnI and inserted into the backbone (3,973 bp) of untagged (686)α_{1S}, from which the sequence encoding (686)α_{1S} had been excised by digestion with HindIII and KpnI. To make (CFP-YFP-686)α_{1S}, the sequence encoding CFP (794 bp) was excised from pECFP-C1 (Clontech Laboratories, Inc.) with NheI and XmaI and ligated into (YFP-686)α_{1S} (see previous paragraph) cleaved with NheI and AgeI (8,243 bp). XmaI and AgeI cleavage sites are compatible for relegation.

α_{1S}(726-CFP-YFP-727). α_{1S}(726-CFP-YFP-727) encodes (in order) (a) α_{1S} residues 1–726, (b) a four-residue linker, (c) CFP–YFP, (d) a 21-residue linker, and (e) α_{1S} residues 727–1,860. CFP-YFP-β_{1a} (Papadopoulos et al., 2004) was cut with AgeI and XmaI. A 1,574-bp fragment encoding the CFP–YFP tandem and the aforementioned linkers were subsequently ligated into the untagged α_{1S} expression vector (Papadopoulos et al., 2004) in which an AgeI recognition sequence was introduced between the triplets encoding Glu^{726} and Ser^{727} via site-directed PCR mutagenesis (QuikChange; Agilent Technologies).

α_{1S}(726-YFP-727). α_{1S}(726-YFP-727) encodes (in order) (a) α_{1S} residues 1–726, (b) a four-residue linker, (c) YFP, (d) a 21-residue linker, and (e) α_{1S} residues 727–1,860. A 786-bp sequence encoding YFP was excised from pEYFP-C1 using AgeI and XmaI. The resultant fragment was ligated into the untagged α_{1S} expression vector in which an AgeI recognition sequence was introduced between the triplets encoding Glu^{726} and Ser^{727} via site-directed PCR mutagenesis.

α_{1S}(760-YFP-761). α_{1S}(760-YFP-761) encodes (in order) (a) α_{1S} residues 1–760, (b) a single-residue linker, (c) YFP, (d) a three-residue linker, and (d) α_{1S} residues 761–1,860. PCR was used to generate a YFP cDNA with 5′ and 3′ NotI restriction sites from pEYFP-N1. The forward primer was 5′-GCGCGCGGCCGCAAATGGTGAGCAAGGGCG-3′, and the reverse primer was 5′-GCGCGCGCGGCCGCTTCTTGTACAGCTCGTCCATGCC-3′. The resultant PCR product was subcloned into a YFP-α_{1S} (Papadopoulos et al., 2004) plasmid that contained a NotI site between the α_{1S} triplets encoding Pro^{760} and Leu^{761} introduced by site-directed mutagenesis with QuikChange primers 5′-GCCCCCGACCGCGGCCGCTGGCCCGAGCTGC-3′ (forward) and 5′-GCAGCTCGGCCAGCGGCCGCGGTCGGGGGC-3′ (reverse). This plasmid was then digested with HindIII and MfeI to excise the segment containing α_{1S}(760-YFP-761), from which the sequence encoding the N-terminal YFP had been removed, and was subcloned into pEYFP-N1 cut with HindIII and MfeI.

α_{1S}(785-YFP-786). α_{1S}(785-YFP-786) encodes (in order) (a) α_{1S} residues 1–785, (b) a four-residue linker, (c) YFP, (d) a 22-residue linker, and (e) α_{1S} residues 786–1,860. PCR was used to generate a YFP/linker cDNA with 5′ and 3′ AgeI restriction sites from α_{1S}(726-YFP-727). The forward primer was 5′-GCGCGCGACCGGTGTCGCCACCATGGTGAGCAAGG-3′, and the reverse primer was 5′-GCGCGCGACCGGTCGGGCCCGCGGTACCGT-3′. An 812-bp PCR product encoding YFP and the aforementioned linkers was subsequently cut with AgeI and ligated into the untagged α_{1S} expression vector in which a GGT triplet (encoding Gly) had been introduced to form a unique AgeI recognition sequence between the triplets encoding Thr^{785} and Asn^{786}. Restriction digests and sequencing were used to verify each cDNA construct.

Expression of cDNA

All procedures involving mice were approved by the University of Colorado Denver Institutional Animal Care and Use Committee. Primary cultures of phenotypically normal (+/+ or +/*mdg*) or dysgenic (*mdg*/*mdg*) myotubes were prepared from newborn mice as described previously (Beam and Franzini-Armstrong, 1997). For electrophysiological experiments, myoblasts were plated into 35-mm plastic culture dishes (Falcon) coated with entactin–collagen IV–laminin (Millipore). Myoblasts destined for immunocytochemistry were plated into 35-mm culture dishes with entactin–collagen IV–laminin–coated glass coverslip bottoms (MatTek). Cultures were grown for 6–7 d in a humidified 37°C incubator with 5% CO_2 in Dulbecco's modified Eagle's medium (Mediatech) supplemented with 10% fetal bovine serum/10% horse serum (Hyclone Laboratories). This medium was then replaced with differentiation medium (Dulbecco's modified Eagle's medium supplemented with 2% horse serum). 2–4 d after the shift to differentiation medium, single nuclei were microinjected with cDNA. For one-piece constructs (α_{1S}(671-CFP-YFP-686), α_{1S}(726-CFP-YFP-727), α_{1S}(726-YFP-727), α_{1S}(760-YFP-761), or α_{1S}(785-YFP-786)), myotubes to be used in electrophysiological experiments were injected with 100 ng/µl cDNA, and myotubes to be immunostained were injected with 60 ng/µl cDNA. For electrophysiology on two-piece constructs, the injection solution contained 60 ng/µl α_{1S}(671) hemichannel cDNA and 100 ng/µl (686)α_{1S} hemichannel cDNA. Only myotubes exhibiting YFP fluorescence were used in experiments.

Measurement of ionic currents

For electrophysiological experiments, myotubes were examined 2 d after injection. Pipettes were fabricated from borosilicate glass and had resistances of ~2.0 MΩ when filled with internal solution, which consisted of 140 mM Cs-aspartate, 10 mM Cs_2-EGTA, 5 mM $MgCl_2$, and 10 mM HEPES, pH 7.4, with CsOH. The standard external solution contained 145 mM TEA-Cl, 10 mM $CaCl_2$, 0.003 mM tetrodotoxin, and 10 mM HEPES, pH 7.4, with TEA-OH. In some experiments, 10 mM $MgCl_2$ was substituted for 10 mM $CaCl_2$ in the external solution. Linear capacitative and leakage currents were determined by averaging the currents elicited by 11 30-mV hyperpolarizing pulses from a holding potential of −80 mV. Test currents were corrected for linear components of leak and capacitive current by digital scaling and subtraction of this average control current. Electronic compensation was used to reduce

TABLE I

α_{1S} fluorescent protein construct conductance and intramembrane charge movement

Construct	*G-V*			*Q-V*			G_{max}/Q'
	G_{max}	$V_{1/2}$	k_G	Q_{max}	V_Q	k_Q	
	nS/nF	*mV*	*mV*	*nC/μF*	*mV*	*mV*	*nS/pC*
α_{1S}-YFP[a]	140 ± 5 (37)	31.2 ± 0.8	8.1 ± 0.2	6.0 ± 0.4 (8)	−3.2 ± 2.0	9.0 ± 0.7	33
α_{1S}(671-CFP-YFP) + (686)α_{1S}	174 ± 13 (20)	36.0 ± 0.9	7.4 ± 0.3	4.2 ± 0.8 (7)	−9.5 ± 4.5	9.2 ± 0.6	54
α_{1S}(671) + (CFP-YFP-686)α_{1S}	144 ± 13 (20)	35.5 ± 1.1	7.8 ± 0.3	3.5 ± 1.4 (4)	−11.1 ± 6.6	9.3 ± 1.4	58
α_{1S}(671-CFP) + (YFP-686)α_{1S}	164 ± 15 (18)	36.0 ± 1.1	7.4 ± 0.4	4.4 ± 1.1 (5)	−4.8 ± 5.4	5.3 ± 2.6	48
α_{1S}(671-CFP-YFP-686)	182 ± 11 (33)	33.9 ± 1.1	7.3 ± 0.3	6.3 ± 0.8 (7)	−3.1 ± 0.8	11.3 ± 0.7	34
α_{1S}(726-CFP-YFP-727)	67 ± 5 (30)[b]	38.5 ± 1.8[d]	10.4 ± 0.7[b]	5.4 ± 0.9 (6)	−12.2 ± 4.1[d]	11.7 ± 1.4	15
α_{1S}(726-YFP-727)	116 ± 11 (15)[b]	35.1 ± 2.2	9.7 ± 0.7[b]	6.9 ± 0.6 (6)	−12.1 ± 1.4[b]	13.4 ± 0.9	20
α_{1S}(760-YFP-761)	102 ± 10 (12)[b]	34.1 ± 0.9	9.2 ± 0.7[c]	8.0 ± 1.6 (5)	−7.6 ± 1.8[c]	14.0 ± 1.4	15
α_{1S}(785-YFP-786)	72 ± 10 (12)[b]	38.9 ± 3.4	9.5 ± 1.7	5.2 ± 0.8 (5)	−11.3 ± 4.8	12.5 ± 1.0	17
Uninjected dysgenic myotubes	no inward current (17)	no inward current (17)	no inward current (17)	1.0 ± 0.2 (6)	−5.0 ± 4.6	9.6 ± 3.0	ND

Data are given as mean ± SEM, with the numbers in parentheses indicating the number of myotubes tested. See Materials and methods for fits. For all of the data given, the calculated average voltage error was <5 mV. Significant differences between α_{1S}(671-CFP-YFP-686) and the other individual one-piece constructs (i.e., α_{1S}(726-CFP-YFP-727), α_{1S}(726-YFP-727), α_{1S}(760-YFP-761), and α_{1S}(785-YFP-786)) are indicated.

[a]α_{1S}-YFP data from Bannister and Beam (2005) are included for comparison.

[b]$P < 0.001$ by *t* test.

[c]$P < 0.01$ by *t* test.

[d]$P < 0.05$ by *t* test.

the effective series resistance (usually to <1 MΩ) and the time constant for charging the linear cell capacitance (usually to <0.5 ms). Ionic currents were filtered at 2 kHz and digitized at 10 kHz. To measure macroscopic L-type current in isolation, a 1-s prepulse to −20 mV followed by a 100-ms repolarization to −50 mV was administered before the test pulse (prepulse protocol; Adams et al., 1990) to inactivate T-type Ca^{2+} channels. Cell capacitance was determined by integration of a transient from −80 to −70 mV using Clampex 8.0 (MDS Analytical Technologies) and was used to normalize current amplitudes (pA/pF). Current–voltage (I-V) curves were fitted using the following equation:

$$I = G_{max} \times (V - V_{rev})/[1 + \exp\{-(V - V_{1/2})/k_G\}], \quad (1)$$

where I is the current for the test potential V, V_{rev} is the reversal potential, G_{max} is the maximum Ca^{2+} channel conductance, $V_{1/2}$ is the half-maximal activation potential, and k_G is the slope factor. All electrophysiological experiments were performed at room temperature (~25°C).

Measurement of intracellular Ca^{2+} transients

Changes in intracellular Ca^{2+} were recorded with Fluo-3 (Invitrogen). The salt form of the dye was added to the standard internal solution for a final concentration of 200 μM. After entry into the whole cell configuration, a waiting period of >5 min was used to allow the dye to diffuse into the cell interior. A 100-W mercury illuminator and a set of fluorescein filters were used to excite the dye present in a small rectangular region of the voltage-clamped myotube. A computer-controlled shutter was used to block illumination in the intervals between test pulses. Fluorescence emission was measured by means of a fluorometer apparatus (Biomedical Instrumentation Group, University of Pennsylvania). The average background fluorescence was quantified before bath immersion of the patch pipette. Fluorescence data are expressed as the total change in fluorescence (ΔF/F), where ΔF represents the change in peak fluorescence from baseline during the test pulse and F is the fluorescence immediately before the test pulse minus the average background (non–Fluo-3) fluorescence. Unless otherwise noted, the peak value of the fluorescence change (ΔF/F) for each test potential (V) was fitted according to

$$\Delta F/F = [\Delta F/F]_{max}/[1 + \exp\{-(V - V_F)/k_F\}], \quad (2)$$

where $(\Delta F/F)_{max}$ is the maximal fluorescence change, V_F is the potential causing half the maximal change in fluorescence, and k_F is a slope parameter. In the cases of α_{1S}(760-YFP-761) and α_{1S}(785-YFP-786), the $\Delta F/F_{max}$-V relationship was fit by

$$\Delta F/F = [\Delta F/F]_{max} \times \exp\{-0.5((V - V_c)/b)^2\}, \quad (3)$$

where $(\Delta F/F)_{max}$ is the maximal fluorescence change and V_c and b are fit parameters (Wilkens and Beam, 2003).

Measurement of charge movements

For measurement of intramembrane charge movements, ionic currents were blocked by the addition of 0.5 mM $CdCl_2$ + 0.1 mM $LaCl_3$ to the standard extracellular recording solution. All charge movements were corrected for linear cell capacitance and leakage currents using a −P/8 subtraction protocol (Bannister et al., 2008a,b). Filtering was at 2 kHz (eight-pole Bessel filter; Frequency Devices, Inc.), and digitization was at 20 kHz. Voltage clamp command pulses were exponentially rounded with a time constant of 50–500 μs, and the prepulse protocol (Adams et al., 1990) was used to reduce the contribution of gating currents from voltage-gated Na^+ channels and T-type Ca^{2+} channels. The integral of the ON transient (Q_{on}) for each test potential (V) was fitted according to

$$Q_{on} = Q_{max}/\{1 + \exp[-(V - V_Q)/k_Q]\}, \quad (4)$$

where Q_{max} is the maximal Q_{on}, V_Q is the potential causing movement of half the maximal charge, and k_Q is a slope parameter.

Electrically evoked contractions

Contractions were elicited by 20-ms, 100-V stimuli applied via an extracellular pipette that contained 150 mM NaCl and was placed near intact myotubes expressing constructs of interest. The myotubes were bathed in Rodent Ringer's solution (146 mM NaCl, 5 mM KCl, 2 mM $CaCl_2$, 1 mM $MgCl_2$, 10 mM HEPES, and 11 mM glucose, pH 7.4, with NaOH). Contractions were assayed by the

movement of an identifiable portion of a myotube across the visual field.

Immunohistochemistry

2 d after the injection, myotubes were washed twice in Ca^{2+}/Mg^{2+}-free Ringer's solution (146 mM NaCl, 5 mM KCl, 10 mM HEPES, and 11 mM glucose, pH 7.4, with NaOH) and fixed in 4% paraformaldehyde solution in PBS (Sigma-Aldrich) for 20 min. Myotubes were then permeabilized with 0.1% Triton X-100/PBS for 30 min. After another PBS wash, nonspecific reactivity was blocked by application of 1% BSA/PBS for 2 h. The primary antibody (mouse anti-α_{1S}, 1:2,000; Thermo Fisher Scientific; also referred to as mAb 1A) was applied overnight at room temperature (~25°C) in a dark, humid environment. The next day, myotubes were again washed with 1% BSA/PBS. The secondary antibody (Alexa Fluor 568–conjugated goat anti–mouse IgG, 1:4,000; Invitrogen) was applied in the dark for 1 h at room temperature. Excess secondary antibody was removed with three 1% BSA/PBS washes. Finally, immunostained myotubes were rinsed with PBS.

Confocal microscopy

Immunostained myotubes were examined in PBS using a confocal laser-scanning microscope (LSM 510 META; Carl Zeiss, Inc.). An area of 500–2,500 μm^2 was selected from the field of view (63× 1.4 NA oil immersion objective), which included the myotube and also an adjacent noncellular region for measurement of background fluorescence. YFP was excited with the 488-nm line of an argon laser (30-mW maximum output, operated at 50% or 6.3 A), and Alexa Fluor 568 was excited with a separate sweep of the 543-nm line from a HeNe laser (1-mW maximum output, operated at 100%), which were directed to the cell via a 488/543-nm dual dichroic mirror. The emitted YFP fluorescence was directed to a photomultiplier equipped with a 505–530 band-pass filter (Chroma Technology Corp.). For Alexa Fluor 568, the emitted fluorescence was directed to a photomultiplier equipped with a 560-nm long-pass filter. Confocal fluorescence intensity data were recorded as the average of four line scans per pixel and digitized at 8 bits, with photomultiplier gain adjusted such that maximum pixel intensities were no more than ~70% saturated.

Analysis

For calculation of G_{max}/Q' ratios, G_{max} was obtained by Eq. 1, whereas Q' was derived by subtracting the average maximal charge movement of dysgenic myotubes (Q_{dys}) from the average total Q_{max}, where Q_{dys} = 1.0 nC/μF (n = 6; Table I). Figures were made using the software program SigmaPlot (version 7.0 or 11.0; SSPS Inc.). All data are presented as mean ± SEM. Statistical comparisons were made by ANOVA or by unpaired, two-tailed t test (as appropriate), with $P < 0.05$ considered significant.

Online supplemental material

Fig. S1 confirms that α_{1S}(726-YFP-727) partially supports skeletal-type EC coupling. Myoplasmic Ca^{2+} transients and L-type currents were recorded with 10 mM Mn^{2+} substituted for 10 mM Ca^{2+} in the bath solution. Online supplemental material is available at http://www.jgp.org/cgi/content/full/jgp.200910241/DC1.

RESULTS

The overall aim of this study was to determine how perturbing the DHPR α_{1S} II–III loop with inserted fluorescent proteins affects bidirectional interactions with RYR1. These constructs are illustrated in Fig. 1 and represent insertions into the peptide A region (Fig. 1, A–D), into the N-terminal portion of the critical domain (Fig. 1, E and F), near the C-terminal edge of the critical domain (Fig. 1 G), and the conserved segment of the α_{1S} II–III loop that intervenes between the critical domain and repeat III (Fig. 1 H).

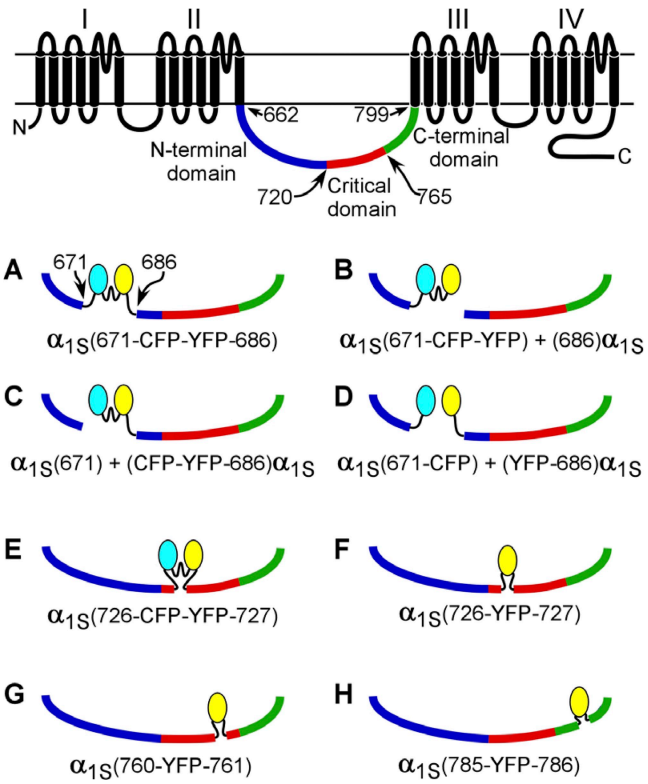

Figure 1. Schematic diagrams of the fluorescent protein α_{1S} fusion constructs. The red segment of the α_{1S} II–III loop represents the EC coupling critical domain (α_{1S} residues 720–765; Nakai et al., 1998b). The linker sequences (see Materials and methods) connecting CFP and YFP to one another and linking the fluorescent proteins to α_{1S} are indicated by wavy lines. (A–D) α_{1S} constructs in which a CFP–YFP tandem was substituted for α_{1S} residues 672–685 (i.e., the tandem replaced the peptide A region). (E and F) α_{1S} constructs in which either the CFP–YFP tandem (E) or a single YFP (F) was introduced between α_{1S} residues 726 and 727. This position lies just inside the N-terminal portion of the critical domain. (G) α_{1S} construct in which YFP was inserted in between residues 760 and 761. This position lies just inside the C-terminal edge of the critical domain. (H) α_{1S} construct in which YFP was inserted between residues 785 and 786. This position lies in the highly conserved C-terminal region of the α_{1S} II–III loop between the critical domain and α_{1S} repeat III.

Insertions into the peptide A region

Previous work monitored the fluorescence resonance energy transfer efficiency of an ~56-kD CFP–YFP tandem inserted in place of the peptide A region of the α_{1S} II–III loop (residues 671–686) as an indicator of spatial environment (Papadopoulos et al., 2004). The fluorescence resonance energy transfer efficiency showed a small dependence on whether or not RYR1 was present when CFP–YFP replaced α_{1S} residues 672–685 in a one-piece construct (Fig. 1 A) but no dependence when the tandem

was fused to the C terminus of an α_{1S} I–II hemichannel (after α_{1S} residue 671) and was coexpressed with an α_{1S} III–IV hemichannel (beginning at α_{1S} residue 686; Fig. 1 B). Thus, in this study, we examined these two constructs in more detail as well as two additional constructs centered on this location. In α_{1S}(671) + (CFP-YFP-686)α_{1S}, the division was made before the tandem (Fig. 1 C), and in α_{1S}(671-CFP) + (YFP-686)α_{1S}, the tandem was split, and the fluorescent proteins resided separately on each hemidomain (Fig. 1 D).

L-type Ca^{2+} currents for the four sets of constructs after expression in dysgenic myotubes are shown in Fig. 2. The one-piece construct α_{1S}(671-CFP-YFP-686) produced large-amplitude L-type Ca^{2+} currents (−6.6 ± 0.5 pA/pF at 50 mV; n = 33) with an I-V relationship ($V_{1/2}$ = 33.9 ± 1.1 mV; Fig. 2 A) that were similar to those reported previously for other fluorescent protein–tagged DHPRs (Table I; Grabner et al., 1998; Wilkens et al., 2001, Flucher et al., 2002; Papadopoulos et al., 2004; Bannister and Beam, 2005; Bannister et al., 2008b). The construct pairs α_{1S}(671-CFP-YFP) + (686)α_{1S} and α_{1S}(671-CFP) + (YFP-686)α_{1S} produced currents similar to those of α_{1S}(671-CFP-YFP-686) in both magnitude (−6.2 ± 0.6 pA/pF [n = 20] and −5.8 ± 0.8 pA/pF [n = 18], respectively; P > 0.05, ANOVA) and voltage dependence (P > 0.05, ANOVA; Table I). The construct pair α_{1S}(671) + (CFP-YFP-686)α_{1S} produced currents with a peak current density (−4.5 ± 0.5 pA/pF at 50 mV; n = 20) slightly lower relative to the other two hemichannel combinations (P > 0.05, ANOVA; Fig. 2 C), despite having similar membrane expression (as assessed by intramembrane charge movement; P > 0.05, ANOVA; Table I). However, it is possible that some of the charge movement for the two-piece constructs was produced by α_{1S} I–II hemidomains unpartnered with α_{1S} III–IV hemidomains (Ahern et al., 2001a; Flucher et al., 2002). Dysgenic myotubes expressing each of the four sets of constructs with the CFP–YFP tandem introduced in place of the peptide A region produced contractions in response to extracellular electrical stimuli (Table II).

Depolarization-triggered myoplasmic Ca^{2+} transients for these constructs are shown in Fig. 3. α_{1S}(671-CFP-YFP-686) triggered robust Ca^{2+} transients ($[\Delta F/F]_{max}$ = 0.69 ± 0.12; n = 7) with an amplitude that had a sigmoidal dependence on test potential (Table II and Fig. 3 A), a signature characteristic of skeletal-type EC coupling (García and Beam, 1994; García et al., 1994). Likewise, α_{1S}(671-CFP-YFP) + (686)α_{1S} ($[\Delta F/F]_{max}$ = 0.61 ± 0.08; n = 9) and α_{1S}(671-CFP) + (YFP-686)α_{1S} ($[\Delta F/F]_{max}$ = 0.93 ± 0.14; n = 7) also served as effective voltage sensors for EC coupling (Table II and Fig. 3, B and D). α_{1S}(671) + (CFP-YFP-686)α_{1S} had a slightly reduced ability to trigger myoplasmic Ca^{2+} release ($[\Delta F/F]_{max}$ = 0.48 ± 0.07; n = 6; P < 0.05, ANOVA; Fig. 3 C and Table II). This slight reduction in ability to mediate EC coupling mirrored the reduced L-type current produced by α_{1S}(671) + (CFP-YFP-686)α_{1S} (Fig. 2 C). However, the main conclusion that can be drawn from the experiments illustrated in Figs. 2 and 3 is that introduction of the CFP–YFP tandem

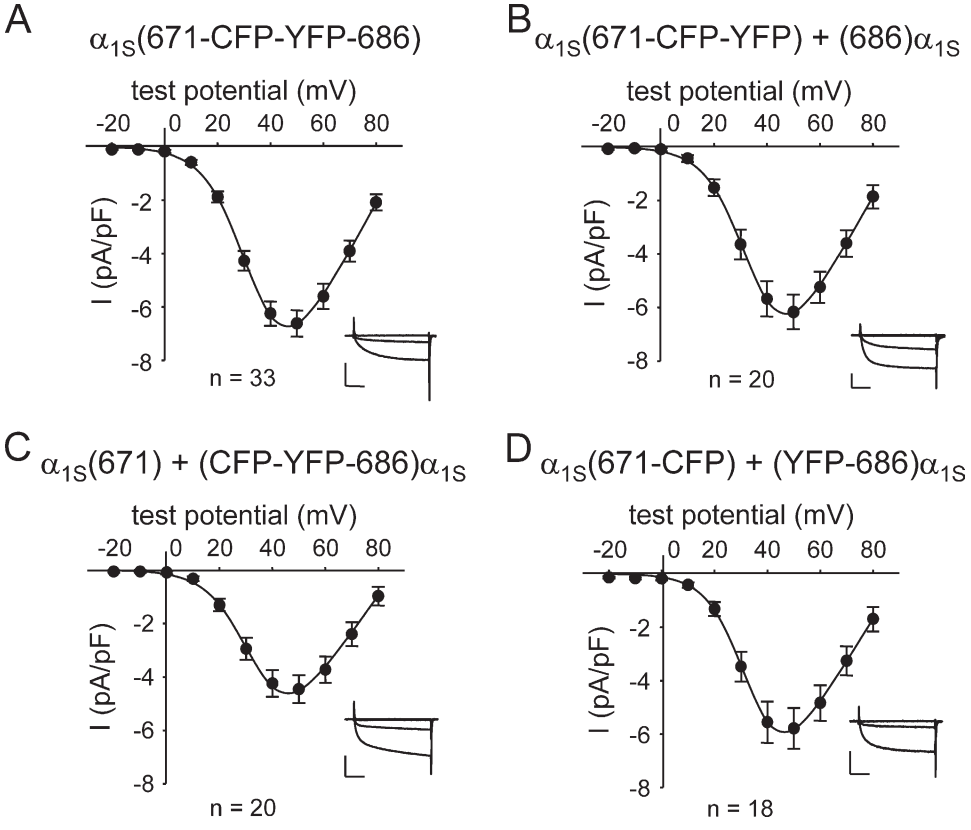

Figure 2. L-type currents are little affected by replacement of α_{1S} residues 672–685 with a CFP–YFP tandem. Peak I-V relationships are shown for dysgenic myotubes expressing α_{1S}(671-CFP-YFP-686) (A), α_{1S}(671-CFP-YFP) + (686)α_{1S} (B), α_{1S}(671) + (CFP-YFP-686)α_{1S} (C), and α_{1S}(671-CFP) + (YFP-686)α_{1S} (D). Currents were evoked at 0.1 Hz by 200-ms test potentials ranging from −20 through 80 mV in 10-mV increments after a prepulse protocol (Adams et al., 1990). Current amplitudes were normalized by linear cell capacitance (pA/pF). Representative current families (test potentials of −20, 0, 20, and 40 mV) for each construct are shown in the insets. Vertical scale bar, 5 pA/pF; horizontal scale bar, 50 ms. The smooth I-V curves are plotted according to Eq. 1, with the best fit parameters for each plot presented in Table I. Error bars represent ±SEM.

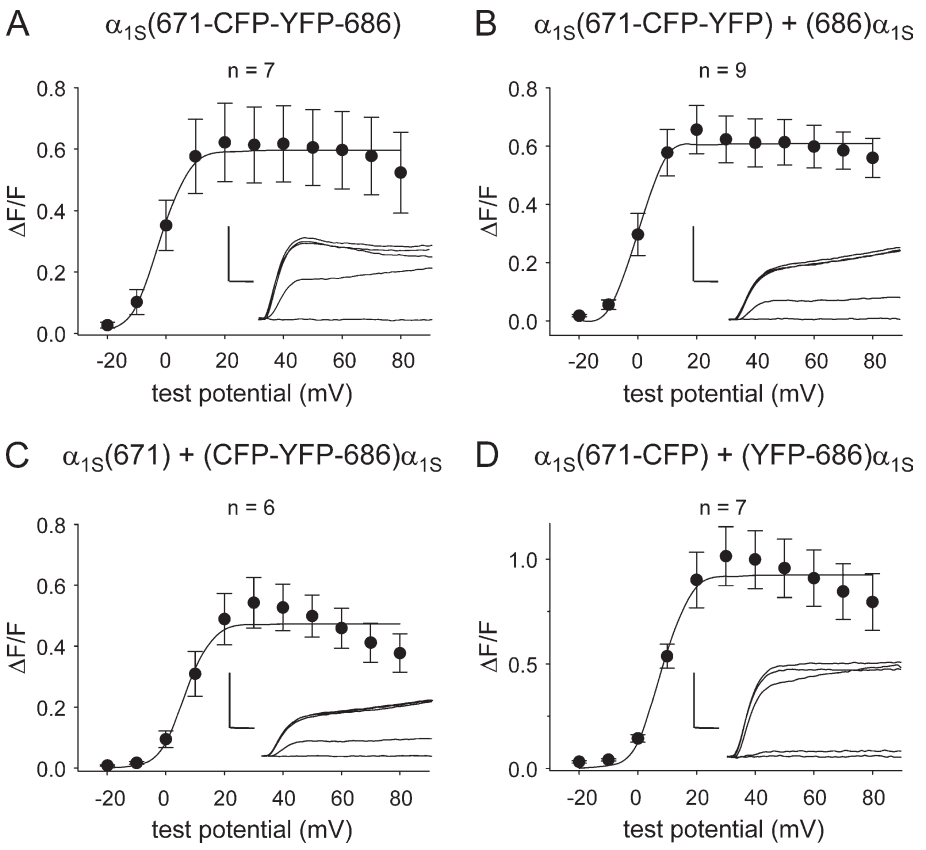

Figure 3. EC coupling is little affected by replacement of α_{1S} residues 672–685 with a CFP–YFP tandem. ΔF/F-V relationships are shown for dysgenic myotubes expressing α_{1S}(671-CFP-YFP-686) (A), α_{1S}(671-CFP-YFP) + (686)α_{1S} (B), α_{1S}(671) + (CFP-YFP-686)α_{1S} (C), and α_{1S}(671-CFP) + (YFP-686)α_{1S} (D). Transients were elicited at 0.1 Hz by 200-ms test potentials ranging from −20 through 80 mV in 10-mV increments after a prepulse protocol (Adams et al., 1990). The smooth ΔF/F-V curves are plotted according to Eq. 2, with the best fit parameters for each plot presented in Table II. Representative transient families (test potentials of −20, 0, 20, 40, and 60 mV) are shown for each construct in the insets. Vertical scale bar, 0.5 ΔF/F; horizontal scale bar, 25 ms. Error bars represent ±SEM.

in place of α_{1S} residues 672–685 had little or no effect on the ability of DHPR to conduct L-type Ca^{2+} current or to support EC coupling.

α_{1S} II–III loop insertions distal to the peptide A region

We next probed the effects of insertions at more C-terminal sites of the loop (Fig. 1, E-H). One obvious

TABLE II

Ability of fluorescent protein-tagged DHPRs to restore EC coupling

Construct	ΔF/F-V			Contracting cells/ number tested
	$[\Delta F/F]_{max}$	V_F	k_F	
		mV	*mV*	
α_{1S}-YFP[a]	0.58 ± 0.09 (15)	6.6 ± 1.6	4.7 ± 0.4	41/47
α_{1S}(671-CFP-YFP) + (686)α_{1S}	0.61 ± 0.08 (9)	0.4 ± 1.5	3.7 ± 0.4	9/11[b]
α_{1S}(671) + (CFP-YFP-686)α_{1S}	0.48 ± 0.07 (6)	7.1 ± 2.0	3.7 ± 0.4	12/15
α_{1S}(671-CFP) + (YFP-686)α_{1S}	0.93 ± 0.14 (7)	7.8 ± 1.5	4.1 ± 0.4	10/25
α_{1S}(671-CFP-YFP-686)	0.69 ± 0.12 (7)	−0.3 ± 2.7	4.9 ± 1.1	26/32
α_{1S}(726-CFP-YFP-727)	No fit (12)	No fit	No fit	0/52
α_{1S}(726-YFP-727)	0.19 ± 0.08 (7)[c]	11.9 ± 3.2[d]	10.0 ± 2.8[d]	5/56
α_{1S}(726-YFP-727) (10 mM Mg^{2+} external)	0.29 ± 0.17 (4)	4.4 ± 6.0	9.1 ± 2.0	ND
α_{1S}(760-YFP-761)	See legend (6)	See legend	See legend	0/72
α_{1S}(785-YFP-786)	No fit (3)	No fit	No fit	0/29
Uninjected dysgenic myotubes	No fit (8)	No fit	No fit	0/100

Data are given as mean ± SEM, with the numbers in parentheses indicating the number of myotubes tested. All ΔF/F-V data given were fit with Eq. 2 except for α_{1S}(760-YFP-761). The ΔF/F-V relationship for α_{1S}(760-YFP-761) was best fit by the Gaussian function $\Delta F/F = [\Delta F/F]_{max} \times \exp\{-0.5(V - V_o/b)^2\}$, where $[\Delta F/F]_{max} = 0.1$, $V_c = 49.2$ mV, and b = 25.7 mV (Eq. 3). "No fit" indicates that the ΔF/F-V relationship could not be well fit by either Eq. 2 or Eq. 3 for the number of myotubes indicated. Significant differences between α_{1S}(671-CFP-YFP-686) and the other individual one-piece constructs that were fit by Eq. 2 (i.e., α_{1S}(726-YFP-727)) are indicated.

[a]α_{1S}-YFP data from Bannister and Beam (2005) are included for comparison.

[b]α_{1S}(671-CFP-YFP) + (686)α_{1S} contraction data were obtained from Papadopoulos et al. (2004).

[c]$P < 0.005$ by *t* test.

[d]$P < 0.05$ by *t* test.

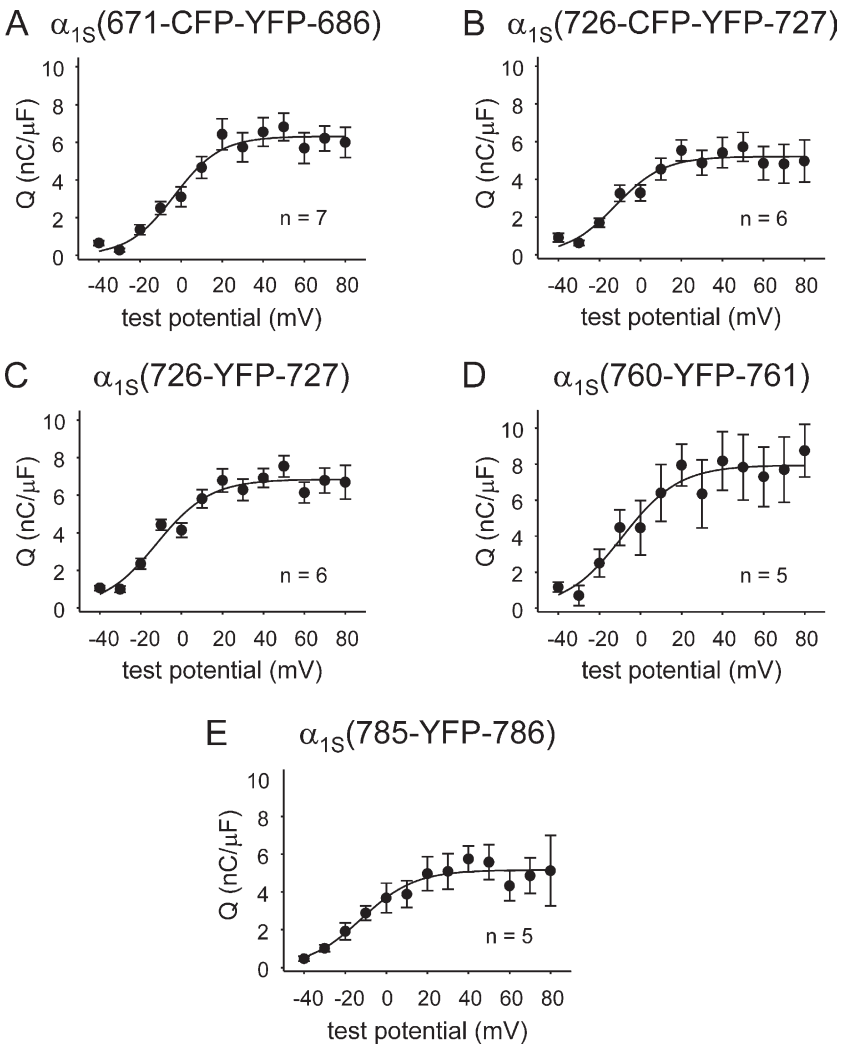

Figure 4. Introduction of fluorescent proteins within either the critical domain or the conserved C-terminal region of the α_{1S} II–III loop does not greatly perturb DHPR membrane expression. Q-V relationships are shown for dysgenic myotubes expressing α_{1S}(671-CFP-YFP-686) (A), α_{1S}(726-CFP-YFP-727) (B), α_{1S}(726-YFP-727) (C), α_{1S}(760-YFP-761) (D), and α_{1S}(785-YFP-786) (E). Charge movements were measured with 20-ms depolarizations from −50 mV in the presence of Cd^{2+} and La^{3+}. Q-V relationships were fit by Eq. 4; the best fit parameters for each plot are presented in Table I. Error bars represent ±SEM.

concern was that these perturbations of the II–III loop might impair expression of the constructs. Thus, we used measurements of membrane-bound charge movements as an indication of membrane expression. These measurements showed that the constructs α_{1S}(726-CFP-YFP-727), α_{1S}(726-YFP-727), α_{1S}(760-YFP-761), and α_{1S}(785-YFP-786) all produced charge movements similar in magnitude to those of α_{1S}(671-CFP-YFP-686) ($P < 0.05$, ANOVA; Table I and Fig. 4, A–E), which was able to mediate robust EC coupling and L-type Ca^{2+} current.

Consequences of fluorescent protein insertion between α_{1S} residues 726 and 727

Based on chimeras of α_{1S} and α_{1C} (Nakai et al., 1998b), residues 720–765 were found to constitute a critical domain for skeletal-type EC coupling, although it is important to note that such chimeric constructs do not allow one to deduce precise boundaries. Indeed, subsequent work with chimeras of α_{1S} and the *Musca domestica* (common house fly) muscle homologue α_{1M} (Kugler et al., 2004b) indicated that skeletal-type EC coupling could be produced by constructs in which α_{1S} residues 720–733 were replaced by nonconserved sequence from α_{1M}. Thus, we sought to determine whether bidirectional signaling would be affected by larger structural perturbations within this region. In contrast to insertion in the peptide A region, insertion of the CFP–YFP tandem between α_{1S} II–III loop residues 726 and 727, α_{1S}(726-CFP-YFP-727), essentially eliminated bidirectional interactions with RYR1 (Fig. 5 A). Thus, α_{1S}(726-CFP-YFP-727) produced currents that were much smaller than those of α_{1S}(671-CFP-YFP-686) (Fig. 5 B and Table I) despite producing similar intramembrane charge movements (Fig. 4, A and B; and Table I). Furthermore, α_{1S}(726-CFP-YFP-727) triggered only barely detectable Ca^{2+} transients in the 12 myotubes examined (Fig. 5 C). Likewise, neither spontaneous nor evoked contractions were observed in dysgenic myotubes expressing α_{1S}(726-CFP-YFP-727) ($n = 52$; Table II).

To determine the effects of introducing a smaller mass at this site, we constructed and characterized an α_{1S} in which a single YFP (~27 kD) was inserted after residue 726 (α_{1S}(726-YFP-727)). In contrast to α_{1S}(726-CFP-YFP-727), partial bidirectional signaling occurred for

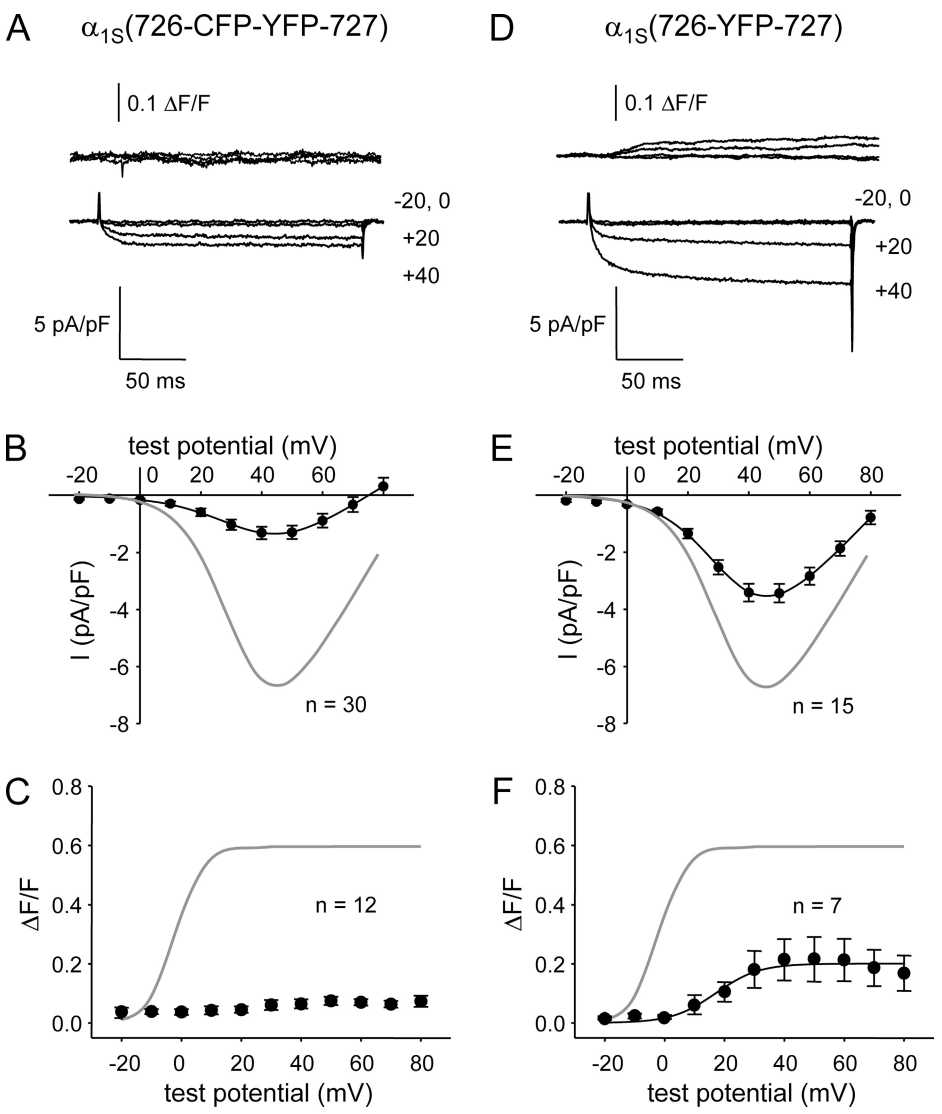

Figure 5. Effect on bidirectional signaling of fluorescent protein insertion between α_{1S} residues 726 and 727. (A and D) Simultaneous recordings of myoplasmic Ca^{2+} transients (top) and L-type Ca^{2+} currents (bottom) elicited by 200-ms depolarizations to the indicated test potentials are shown for dysgenic myotubes expressing either α_{1S}(726-CFP-YFP-727) (A) or α_{1S}(726-YFP-727) (D). (B and E) I-V relationships are shown for α_{1S}(726-CFP-YFP-727) and α_{1S}(726-YFP-727) in B and E, respectively. The gray lines represent the average I-V relationship for α_{1S}(671-CFP-YFP-686). (C and F) ΔF/F-V relationships for α_{1S}(726-CFP-YFP-727) and α_{1S}(726-YFP-727) are shown in C and F, respectively. The gray lines represent the average ΔF/F-V relationship for α_{1S}(671-CFP-YFP-686). The best fit parameters for the data in each panel are presented in Tables I and II. Error bars represent ±SEM.

α_{1S}(726-YFP-727) (Fig. 5 D), although this signaling was compromised compared with α_{1S}(671-CFP-YFP-686). Thus, L-type current density was more than twofold larger than for α_{1S}(726-CFP-YFP-727), although not as large as for α_{1S}(671-CFP-YFP-686) (Fig. 5 E and Table I). Moreover, α_{1S}(726-YFP-727) supported modest myoplasmic Ca^{2+} transients ($[\Delta F/F]_{max} = 0.19 \pm 0.08$; $n = 7$; Fig. 5 F and Table II), which displayed a sigmoidal voltage dependence that was positively shifted (10–20 mV) relative to α_{1S}(671-CFP-YFP-686). A small number of evoked contractions were observed in dysgenic myotubes expressing α_{1S}(726-YFP-727) (5 of 56 myotubes tested; Table II).

Although the sigmoidal voltage dependence of the Ca^{2+} transients (Fig. 5 F) suggested that the modest Ca^{2+} release observed for α_{1S}(726-YFP-727) was skeletal type, we further tested the nature of this release by equimolar substitution of Mg^{2+} for Ca^{2+} in the external solution. Substitution of Mg^{2+} for Ca^{2+} had little effect on either the magnitude ($[\Delta F/F]_{max} = 0.29 \pm 0.17$; $n = 4$; $P > 0.05$, t test) or the sigmoidal voltage dependence of SR Ca^{2+} release (Fig. S1). These results indicate that bidirectional coupling was partially restored by α_{1S}(726-YFP-727), although both orthograde and retrograde coupling were impaired.

Bidirectional coupling with RYR1 is disrupted in α_{1S}(760-YFP-761)

With the knowledge that the triad junction can accommodate insertion of a single YFP near the N-terminal boundary of the critical domain, we next tested whether introduction of YFP near the C-terminal boundary of this region, α_{1S}(760-YFP-761), would also partially spare bidirectional signaling. This construct produced small Ca^{2+} currents and transients (Fig. 6 A). On average, α_{1S}(760-YFP-761) produced Ca^{2+} currents that were about half the magnitude of those for α_{1S}(671-CFP-YFP-686) (Fig. 6 B). However, α_{1S}(760-YFP-761) produced somewhat larger charge movements than the other clones examined (Fig. 4 and Table I). If this increased membrane expression is taken into account, the magnitude of the currents produced by α_{1S}(760-YFP-761) differed little from those of

α_{1S}(726-CFP-YFP-727) (Fig. 5 B), as indicated by their equivalent G_{max}/Q' ratios (Table I).

Depolarization-elicited Ca^{2+} transients were detectable in dysgenic myotubes expressing α_{1S}(760-YFP-761) ($[\Delta F/F]_{max} = 0.10 \pm 0.02$; $n = 6$; Fig. 6 A). However, these small transients appeared to be a consequence of Ca^{2+} entry via the L-type current because the $\Delta F/F$-V relationship (Fig. 6 C) did not display the sigmoidal shape expected for skeletal-type EC coupling but instead mirrored the peak I-V relationship (Fig. 6 B). No spontaneous or evoked contractions were observed in dysgenic myotubes expressing α_{1S}(760-YFP-761) ($n = 72$; Table II). Thus, it appears that both orthograde and retrograde signaling are largely ablated by insertion of YFP between α_{1S} II–III loop residues 760 and 761.

Bidirectional coupling with RYR1 is also disrupted in α_{1S}(785-YFP-786)

An important limitation of the analysis of chimeras of α_{1C} or α_{1M} with α_{1S} is that the region corresponding to α_{1S} residues 773–799 is quite well conserved between the three α_1 subunits (Wilkens et al., 2001). Thus, the chimeras are not informative about the potential importance of this region. Therefore, we directly probed this region by inserting YFP between α_{1S} residues 785 and 786 (α_{1S}(785-YFP-786)). Dysgenic myotubes expressing α_{1S}(785-YFP-786) produced minimal Ca^{2+} currents and transients (Fig. 7 A). Thus, current density for α_{1S}(785-YFP-786) was very low (-1.4 ± 0.4 pA/pF at 40 mV; $n = 12$; Fig. 7 B), although it produced charge movements ($Q_{max} = 5.2 \pm 0.8$ nC/μF; $n = 5$; Fig. 4 E) that were similar to those of the other one-piece constructs that supported bidirectional signaling (Fig. 4, A and C; and Table I). The G_{max}/Q' ratio for α_{1S}(785-YFP-786) was similar to that of α_{1S}(726-CFP-YFP-727) and α_{1S}(760-YFP-761) (Table I).

In addition to eliminating retrograde coupling, insertion of YFP between α_{1S} residues 785 and 786 also abolished orthograde coupling, as Ca^{2+} transients were nearly undetectable (Fig. 7 C). No spontaneous or evoked contractions were observed in dysgenic myotubes expressing α_{1S}(785-YFP-786) ($n = 29$; Table II). These results indicate that insertion of a single fluorescent protein between α_{1S} residues 785 and 786 disrupts bidirectional coupling.

Insertion of fluorescent proteins does not impede antibody binding to the critical domain

Within the critical domain, α_{1S} residues 737–744 are recognized by mAb 1A, and mutations within this region were shown to have parallel effects on the immunohistochemical binding of the antibody and on orthograde coupling (Kugler et al., 2004a). On the basis of this result, it was hypothesized that the appropriate conformation of α_{1S} residues 737–744 is essential for communication between DHPR and RYR1. Thus, we used the strategy

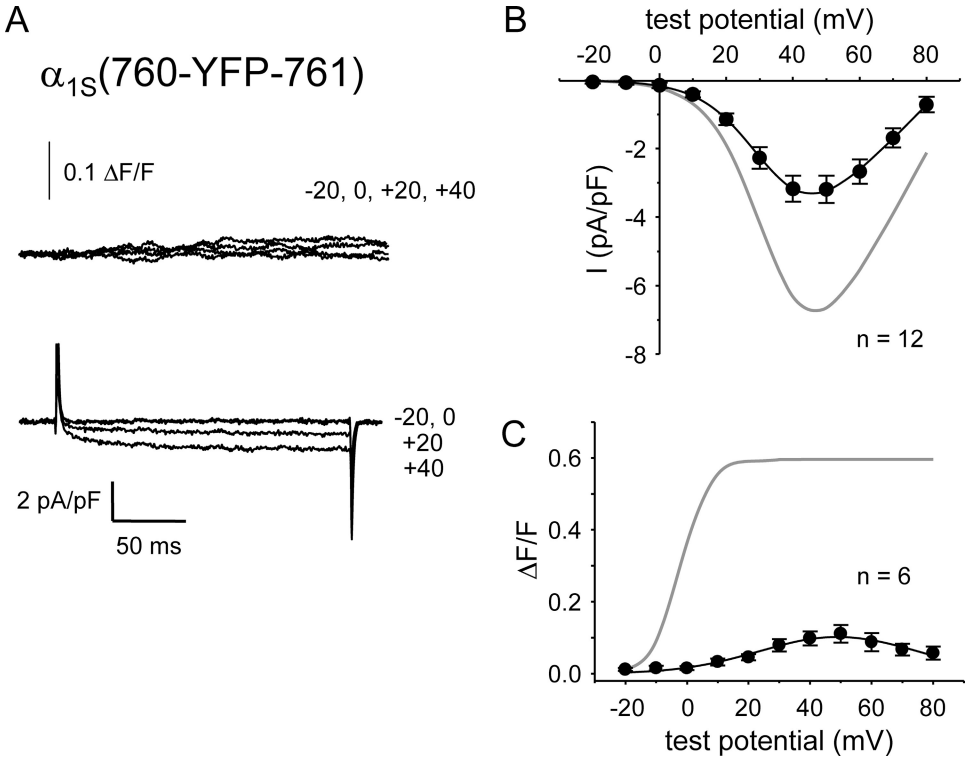

Figure 6. Bidirectional signaling is disrupted by insertion of YFP between α_{1S} residues 760 and 761. (A) Simultaneous recordings of myoplasmic Ca^{2+} transients (top) and L-type Ca^{2+} currents (bottom) elicited by 200-ms depolarizations to the indicated test potentials are shown for a dysgenic myotube expressing α_{1S}(760-YFP-761). Note the large charge movement relative to small L-type currents and Ca^{2+} transients. (B) I-V relationship for α_{1S}(760-YFP-761). The gray line represents the average I-V relationship for α_{1S}(671-CFP-YFP-686). (C) Voltage dependence of Ca^{2+} transients from dysgenic myotubes expressing α_{1S}(760-YFP-761). The smooth curve for the α_{1S}(760-YFP-761) data represents $\Delta F/F = [\Delta F/F]_{max} \times \exp\{-0.5(V - V_o/b)^2\}$, where $[\Delta F/F]_{max} = 0.1$, $V_c = 49.2$ mV, and $b = 25.7$ mV (Eq. 3). The gray line represents the $\Delta F/F$-V relationship for α_{1S}(671-CFP-YFP-686). Myoplasmic Ca^{2+} transients were recorded only from myotubes that had quantifiable L-type current. Error bars represent ±SEM.

illustrated in Fig. 8 A to test whether mAb 1A could recognize its epitope in the constructs with impaired bidirectional coupling (i.e., α_{1S}(726-CFP-YFP-727), α_{1S}(726-YFP-727), α_{1S}(760-YFP-761), and α_{1S}(785-YFP-786); Figs. 5–7). Fig. 8 B shows for YFP-α_{1S} that the yellow fluorescence (middle, green) and mAb 1A staining (top, red) colocalize in discrete puncta (bottom, yellow). Similarly colocalized puncta of yellow fluorescence and mAb 1A staining were also observed for α_{1S}(726-CFP-YFP-727), α_{1S}(726-YFP-727), α_{1S}(760-YFP-761), and α_{1S}(785-YFP-786) (Fig. 8, C–F). Such puncta were completely absent in dysgenic myotubes not injected with α_{1S} cDNAs (unpublished data). Furthermore, in control experiments in which the primary antibody was omitted, red puncta were absent despite the persistence of puncta generated by YFP fluorescence (unpublished data). Previous work has demonstrated that DHPR puncta in myotubes colocalize with RYR1 (Takekura et al., 2004). Thus, the data in Fig. 8 support the idea that each of the fluorescent protein α_{1S} constructs was efficiently targeted to plasma membrane junctions with the SR. In addition, these data demonstrate that the introduction of either a single YFP or a CFP–YFP tandem did not severely disrupt the conformation of the antibody epitope within the critical domain.

DISCUSSION

In this study, we have evaluated the effects of fluorescent protein insertion as a tool for obtaining information about domains of the α_{1S} II–III loop (residues 662–799) that are essential for bidirectional coupling with RYR1. The insertions were at four sites: (1) replacing residues 672–685 within the peptide A region, (2) between residues 726 and 727 near the N-terminal boundary of the critical domain (residues 720–765), (3) between residues 760 and 761 near the C-terminal boundary of the critical domain, and (4) between residues 785 and 786 in the conserved C-terminal region of the α_{1S} II–III loop. Bidirectional coupling between DHPR and RYR1 displayed a differential sensitivity to insertions at these four sites. This coupling was unaffected by insertion of a large (~56 kD) CFP–YFP tandem in place of the peptide A region but was ablated by the same insertion between α_{1S} residues 726 and 727. Bidirectional coupling was partially spared by insertion of only a single fluorescent protein (YFP) between α_{1S} residues 726 and 727 but totally eliminated by insertion either between α_{1S} residues 760 and 761 or between residues 785 and 786.

Each of the α_{1S} tandem constructs in which the CFP–YFP tandem was substituted for α_{1S} residues 672–685 (Fig. 1, A–D) functioned normally both as a voltage-gated Ca^{2+} channel and as a voltage sensor for EC coupling (Figs. 2 and 3) regardless of whether the α_{1S} construct was expressed as a combination of two hemidomains (α_{1S} repeats I–II and repeats III–IV) or as an intact channel. This finding is in agreement with several previous studies demonstrating that EC coupling is unaffected by scrambling, deleting, or substituting unrelated sequence for the peptide A region of the α_{1S} II–III loop (Proenza et al., 2000b; Ahern et al., 2001a,b; Wilkens et al., 2001; Flucher et al., 2002; Lorenzon et al., 2004; Papadopoulos

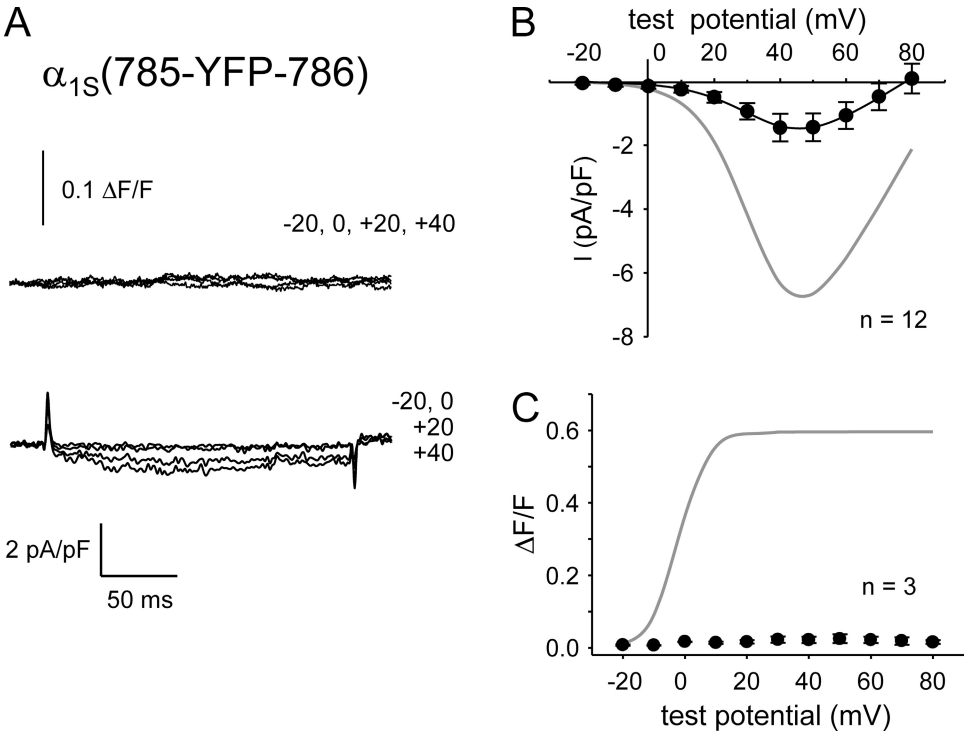

Figure 7. Bidirectional signaling is disrupted by insertion of YFP between α_{1S} residues 785 and 786. (A) Simultaneous recordings of myoplasmic Ca^{2+} transients (top) and L-type Ca^{2+} currents (bottom) elicited by 200-ms depolarizations to the indicated test potentials are shown for a dysgenic myotube expressing α_{1S}(785-YFP-786). (B) I-V relationship for α_{1S}(785-YFP-786). The gray line represents the average I-V relationship for α_{1S}(671-CFP-YFP-686). (C) Lack of Ca^{2+} transients in dysgenic myotubes expressing α_{1S}(785-YFP-786). The gray line represents the average ΔF/F-V relationship for α_{1S}(671-CFP-YFP-686). Myoplasmic Ca^{2+} transients were recorded only from myotubes that had quantifiable L-type current. Error bars represent ±SEM.

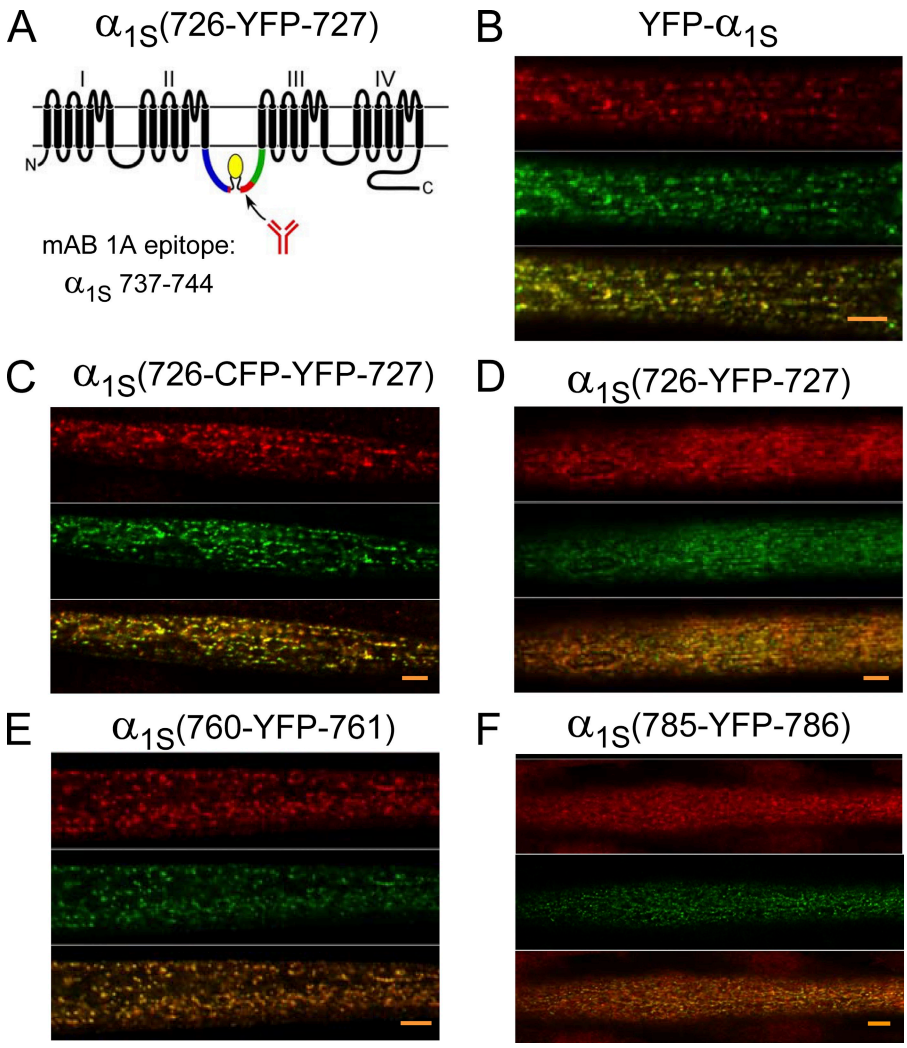

Figure 8. Insertion of fluorescent protein at residues 726, 760, or 785 within the α_{1S} II–III loop does not interfere with recognition of the critical domain by a site-specific mAb. (A) Schematic representation of α_{1S} and the epitope recognized by mAb 1A (residues 737–744; Kugler et al., 2004a). α_{1S}(726-YFP-727) is shown as an arbitrary example. (B–F) Confocal fluorescence images of mAb 1A binding (top, red), α_{1S} fluorescent protein distribution (middle, green), and the overlay of the antibody binding and α_{1S} distribution (bottom) are shown for dysgenic myotubes expressing YFP-α_{1S} (B), α_{1S}(726-CFP-YFP-727) (C), α_{1S}(726-YFP-727) (D), α_{1S}(760-YFP-761) (E), and α_{1S}(785-YFP-786) (F). The images represent optical sections near the myotube surface. In deeper optical sections, the overlapping red and yellow puncta were largely absent from the core of the myotube and were present only at the periphery (not depicted). Alexa Fluor 568–conjugated anti–mouse IgG was used to visualize the binding of mAb 1A. Bars, 5 µm.

et al., 2004; Lorenzon and Beam, 2007). Clearly, these previous results had already indicated that the binding of the peptide A region to other junctional proteins is unnecessary for coupling with RYR1. It now seems possible to broaden this conclusion. First, the ability of the peptide A region to accommodate the CFP–YFP tandem, together with this region's accessibility to a large (~60 kD) streptavidin probe (Lorenzon et al., 2004; Lorenzon and Beam, 2007), suggests that the segments of the α_{1S} II–III loop adjacent to the peptide A region are also fully exposed to the myoplasm at the triad junction and thus devoid of junctional interaction partners in both resting and depolarized cells. Second, it seems extremely unlikely that peptide A and/or immediately adjacent regions of the α_{1S} II–III loop are important for propagating signaling-related conformational changes to RYR1 because one might expect such conformational changes to be impeded by the presence of the CFP–YFP tandem.

Unlike insertions in the peptide A region, insertions of fluorescent protein in either the N- or C-terminal portions of the critical domain of the α_{1S} II–III loop significantly impacted bidirectional signaling. To evaluate these effects, it is useful to consider the landmarks of the critical domain. This region was initially characterized as α_{1S} residues 720–765 on the basis of functional analysis of chimeras between α_{1S} and α_{1C} (Nakai et al., 1998b). The top portion of Fig. 9 compares the sequence of these 46 α_{1S} residues (720–765) with the corresponding residues of α_{1C} (851–896) and α_{1M} (712–756). Subsequent work identified a slightly smaller region of 31 α_{1S} residues that was sufficient to restore full bidirectional signaling when inserted into a II–III loop otherwise having an α_{1M} sequence (chimera $SkLMS_{31}$; Kugler et al., 2004b). Fig. 9 illustrates the position of this slightly smaller segment of the critical domain and also compares the sequences of α_{1S}, α_{1C}, and α_{1M} that extend from the C-terminal edge of the critical domain to the beginning of repeat IIIS1.

Insertion of the tandem within the N-terminal portion of the critical domain abolished bidirectional signaling (Fig. 5, A–C). This loss of signaling did not appear to be a consequence of loss of membrane expression because charge movements for α_{1S}(726-CFP-YFP-727) were not

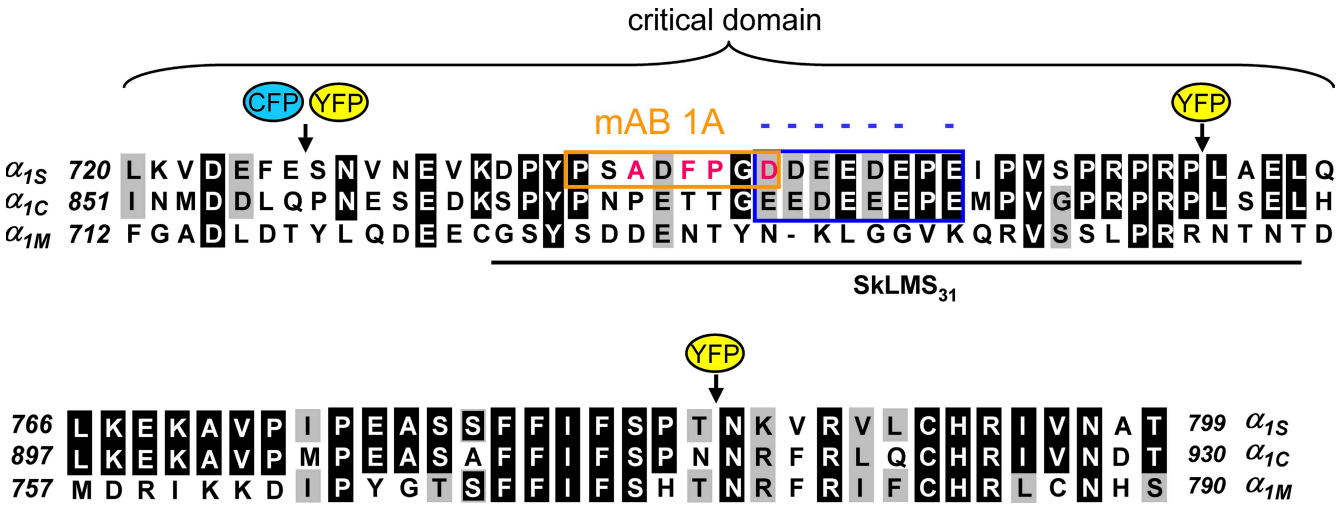

Figure 9. Sequence comparison of the critical domain and C-terminal region of the α_{1S} II–III loop with the corresponding regions of α_{1C} and α_{1M}. Sequence alignment is shown for rabbit α_{1S} (GenBank/EMBL/DDBJ accession no. X05921), rabbit α_{1C} (GenBank/EMBL/DDBJ accession no. X15539), and *M. domestica* α_{1M} (GenBank/EMBL/DDBJ accession no. Z31723). The top panel (α_{1S} residues 720–765) represents the critical domain as defined by Nakai et al. (1998b). The bottom panel (α_{1S} residues 766–799) represents the region of the II–III loop C-terminal to the critical domain, ending just before repeat III (Tanabe et al., 1987). Sequence is not shown for the relatively divergent N-terminal portion of the II–III loop (α_{1S} residues 662–719). Residues of α_{1C} or α_{1M} identical to those of α_{1S} are shaded in black, and residues conserved with those of α_{1S} are shaded in gray. For the SkLMS$_{31}$ chimera (Kugler et al., 2004b), the black line indicates α_{1S} sequence inserted into the *M. domestica* loop. The epitope for binding of mAb 1A (Kugler et al., 2004a) is boxed in orange. The conserved α_{1S}/α_{1C} negative charge cluster is boxed in blue. Individual point mutation of any of the nonconserved α_{1S} residues indicated in red to the corresponding α_{1C} residues results in a decreased magnitude of skeletal-type EC coupling (Kugler et al., 2004b) and loss of mAb 1A binding (Kugler et al., 2004a). Black arrows indicate the positions of fluorescent protein insertion for α_{1S}(726-CFP-YFP-727), α_{1S}(726-YFP-727), α_{1S}(760-YFP-761), or α_{1S}(785-YFP-786) (Fig. 1).

significantly different from those of α_{1S}(671-CFP-YFP-686) (Fig. 4, A and B; and Table I). Additionally, junctional targeting, as indicated by fluorescent puncta near the surface, appeared to be normal for α_{1S}(726-CFP-YFP-727) (Fig. 8 C). Thus, it appears that tandem insertion between residues 726 and 727 specifically eliminated interaction with RYR1 because Ca^{2+} transients were absent and the currents for α_{1S}(726-CFP-YFP-727) had amplitude and kinetics like those of Ca^{2+} current in dyspedic myotubes, where RYR1 is genetically absent (Nakai et al., 1996, 1998a; Avila and Dirksen, 2000; Sheridan et al., 2006). One possibility for why bidirectional coupling is absent for α_{1S}(726-CFP-YFP-727) is that the insertion of the tandem between residues 726 and 727 severed a sequence of the loop that binds to other junctional proteins. However, substantial alteration of the primary sequence surrounding α_{1S} residues 726 and 727, as occurs in the chimera SkLMS$_{31}$ (Fig. 9), appears to have no effect on bidirectional signaling (Kugler et al., 2004b). Another argument against the idea that interruption of the primary sequence accounts for the complete loss of coupling by α_{1S}(726-CFP-YFP-727) is that coupling was partially preserved in the construct α_{1S}(726-YFP-727), as shown in Fig. 5 (D–F).

Compared with the N-terminal edge of the critical domain, the C-terminal edge appeared more sensitive to introduction of a single fluorescent protein. Thus, weak bidirectional signaling was present for the construct α_{1S}(726-YFP-727) but was completely absent for the construct α_{1S}(760-YFP-761). It should be noted that the YFP connecting linkers were substantially shorter for the insertion between residues 760/761 than for the insertion between residues 726/727 (see Materials and methods). Although the different linker length could have contributed to the greater effect of YFP insertion at residues 760/761 than at residues 726/727, it seems unlikely to account for the much greater effect of YFP insertion at residues 785/786 compared with residues 726/727 because the linker lengths were nearly identical at the two positions. Thus, it seems reasonable to conclude that bidirectional signaling is much more sensitive to perturbation at residues 785/786 than at residues 726/727.

The suppression of bidirectional signaling produced by inserting fluorescent proteins within the N- or C-terminal portions of the critical domain could, in principle, result from disruption of the tertiary structure of this entire region. However, the structure of this region did not appear to be severely altered because mAb 1A was able to recognize its epitope (α_{1S} residues 737–744) within the critical domain of the constructs α_{1S}(726-CFP-YFP-727), α_{1S}(726-YFP-727), α_{1S}(760-YFP-761), and α_{1S}(785-YFP-786) (Fig. 8, C–F).

The absence of bidirectional signaling for α_{1S}(726-CFP-YFP-727) and α_{1S}(760-YFP-761) is consistent with the idea that the binding of α_{1S} residues (727–760) to other junctional proteins (e.g., RYR1) is necessary for functional coupling. For example, one could hypothesize

that voltage sensor movement in response to depolarization promotes a conformation of the α_{1S} II–III loop that favors the bound state of this region of the critical domain and, thus, both SR Ca^{2+} release and retrograde signaling. If this model were correct, the addition of the extra mass of fluorescent protein near either the N- or C-terminal boundaries of the critical domain could slow the on-rate for binding, shift the equilibrium toward the unbound state, and thus reduce the magnitude of bidirectional coupling. This kinetic model would explain why the CFP–YFP tandem with its greater mass had a larger effect when inserted after residue 726 than did YFP alone. A second hypothesis (occlusion model) is that the presence of the fluorescent proteins sterically occludes entry of α_{1S} II–III loop residues into a binding pocket. According to this model, the binding of residues 727–760 would be completely occluded by the presence of the CFP–YFP tandem between residues 726–727 but only partially occluded by a single YFP at this position.

Either the kinetic or occlusion model could be made compatible with the observation that bidirectional coupling was totally absent for α_{1S}(760-YFP-761). With the kinetic model, for example, it could be postulated that the C-terminal segment of the α_{1S} II–III loop (roughly from residue 760 to repeat III) is essential for coupling between voltage sensor movement and the active conformation of the critical domain and that this coupling is drastically slowed by the presence of fluorescent protein between α_{1S} residues 760 and 761. Alternatively, the YFP placed between α_{1S} residues 760 and 761 might directly interfere with the binding of the adjacent critical domain residues to other junctional proteins.

Whether or not these aforementioned specific hypotheses have validity, it is important to recognize that the region of the α_{1S} II–III loop downstream from the critical domain is well conserved between α_{1S}, α_{1C}, and α_{1M} (Fig. 9, bottom), which means that its importance has not been previously tested by chimeras between these channels. In this regard, the ablation of both orthograde and retrograde coupling by introduction of YFP between α_{1S} residues 785 and 786 (Fig. 7) clearly indicates that the integrity of this region is vital for skeletal-type EC coupling. It remains to be determined whether this domain functions as a conduit for intramolecular communication between the voltage sensor and the critical domain or whether it serves as a site for intermolecular interactions that support bidirectional communication between DHPR and RYR1.

In addition to functional evidence for the importance of the critical domain of the α_{1S} II–III loop, yeast two-hybrid assays have revealed a weak interaction between the critical domain and a segment of RYR1 (residues 1,837–2,168; Proenza et al., 2002). Freeze-fracture electron microscopy also provides structural evidence that the critical domain of the α_{1S} II–III loop is important for linking DHPRs to RYR1. In particular, the arrangement of DHPRs into tetrads depends on the presence of RYR1 in the SR at sites of junction with the plasma membrane (Protasi et al., 1998, 2000, 2002). Tetrads are not formed upon expression in dysgenic myotubes of a chimera consisting of α_{1S} with a II–III loop having an α_{1C} sequence (SkLC), but tetrads are formed when the critical domain portion of the loop of SkLC is converted back to an α_{1S} sequence (Takekura et al., 2004). Interestingly, however, relatively good tetrad formation was observed for a chimera (SkLM) consisting of α_{1S} with a II–III loop having an α_{1M} sequence (Takekura et al., 2004), even though this construct did not support skeletal-type EC coupling (Wilkens et al., 2001).

Ahern et al. (2001b) found that a one-piece α_{1S} construct lacking the critical domain did not mediate skeletal-type EC coupling, but a construct lacking both the critical domain and the peptide A region did support weak coupling, producing maximal transients of ~15% of the amplitude of wild-type α_{1S}. Thus, in addition to the critical domain, other regions of the DHPR have some ability to participate in the interactions that support EC coupling. The organization of SkLM into tetrads (Takekura et al., 2004) also implies that yet-to-be-identified regions of the DHPR must participate in the interactions linking the DHPR to RYR1. Our present results (Figs. 2–7) raise the possibility that one of these yet-to-be-identified regions is the portion of the α_{1S} II–III loop that is C-terminal to the critical domain (Fig. 9, bottom).

In addition to the critical domain and C-terminal region of the α_{1S} II–III loop, other DHPR domains are also possible sites involved in coupling to RYR1. For example, the C-terminal region of β_{1a} strongly influences bidirectional signaling (Beurg et al., 1999; Sheridan et al., 2003a,b, 2004; García et al., 2005). β_{1a} also facilitates tetrad formation, as the β_{1a}-null zebrafish mutant relaxed lacks the characteristic orthogonal DHPR arrays typically observed in freeze-fracture replicas of normal skeletal muscle (Schredelseker et al., 2005, 2008). Other possible sites that may interact with RYR1 are the α_{1S} III–IV loop (Leong and MacLennan, 1998b; but see Bannister et al., 2008b) and proximal portions of the C terminus of α_{1S} (Slavik et al., 1997; Flucher et al., 2000; Proenza et al., 2000a; Sencer et al., 2001; Lorenzon et al., 2004; Papadopoulos et al., 2004; Lorenzon and Beam, 2007).

Overall, the effects of inserting fluorescent proteins into the α_{1S} II–III loop are consistent with the idea that binding of the α_{1S} II–III loop critical domain to other junctional proteins is important for bidirectional signaling. Our current results expand our knowledge of the mechanism of bidirectional coupling by identifying the importance of the conserved region of the α_{1S} II–III loop that connects the critical domain to α_{1S} repeat III. However, our results do not exclude roles for other regions of the DHPR that have been implicated as involved in coupling with RYR1. Indeed, it seems quite likely that several cytoplasmic regions of the DHPR, in addition to

those already implicated, participate in interactions that positively or negatively influence coupling between the DHPR and RYR1 (Bannister, 2007). However, we are now in a position to exclude at least a couple of regions from likely involvement. One such region is the N terminus of α_{1S}, which can be largely deleted without affecting function (Bannister and Beam, 2005). Based on both previous results (Proenza et al., 2000b; Ahern et al., 2001a,b; Flucher et al., 2002; Lorenzon et al., 2004; Papadopoulos et al., 2004; Lorenzon and Beam, 2007) and those described in this study, it also seems possible to exclude the involvement of peptide A and adjacent regions of the N-terminal portion of the α_{1S} II–III loop as an essential trigger for EC coupling.

The fact that gating of RYR1 is responsive to voltage across the plasma membrane means that the functional state of the DHPR must control the conformation of at least some of the cytoplasmic DHPR regions important for coupling. Regions of this sort may be difficult to define by standard biochemical or structural approaches. Thus, it is likely to continue to be of value to use the kinds of approaches described here to probe the importance of other cytoplasmic domains of the DHPR.

We thank current and former members of the Beam laboratory for insightful discussion.

This work was supported in part by National Institutes of Health (NIH) grants AR055104 and AR44750 (to K.G. Beam), a grant from the Muscular Dystrophy Association (MDA4319 to K.G. Beam), and Deutsche Forschungsgemeinschaft grant PA801/2-1 (to S. Papadopoulos). R.A. Bannister was supported by NIH training grant NS543115 and by a developmental grant from the Muscular Dystrophy Association (MDA4155).

Edward N. Pugh Jr. served as editor.

Submitted: 9 April 2009
Accepted: 9 June 2009

REFERENCES

Adams, B.A., T. Tanabe, A. Mikami, S. Numa, and K.G. Beam. 1990. Intramembrane charge movement restored in dysgenic skeletal muscle by injection of dihydropyridine receptor cDNAs. *Nature.* 346:569–572.

Ahern, C.A., J. Arikkath, P. Vallejo, C.A. Gurnett, P.A. Powers, K.P. Campbell, and R. Coronado. 2001a. Intramembrane charge movements and excitation-contraction coupling expressed by two-domain fragments of the Ca^{2+} channel. *Proc. Natl. Acad. Sci. USA.* 98:6935–6940.

Ahern, C.A., D. Bhattacharya, L. Mortenson, and R. Coronado. 2001b. A component of excitation-contraction coupling triggered in the absence of the T671-L690 and L720-Q765 regions of the II-III loop of the dihydropyridine receptor α_{1S} pore subunit. *Biophys. J.* 81:3294–3307.

Ahern, C.A., D.C. Sheridan, W. Cheng, L. Mortenson, P. Nataraj, P.D. Allen, M. De Waard, and R. Coronado. 2003. Ca^{2+} current and charge movements in skeletal myotubes promoted by the β-subunit of the dihydropyridine receptor in the absence of ryanodine receptor type 1. *Biophys. J.* 84:942–959.

Avila, G., and R.T. Dirksen. 2000. Functional impact of the ryanodine receptor on the skeletal muscle L-type Ca^{2+} channel. *J. Gen. Physiol.* 115:467–480.

Avila, G., K.M. O'Connell, L.A. Groom, and R.T. Dirksen. 2001. Ca^{2+} release through ryanodine receptors regulates skeletal muscle L-type Ca^{2+} channel expression. *J. Biol. Chem.* 276:17732–17738.

Bannister, R.A. 2007. Bridging the myoplasmic gap: recent developments in skeletal muscle excitation-contraction coupling. *J. Muscle Res. Cell Motil.* 28:275–283.

Bannister, R.A., and K.G. Beam. 2005. The α_{1S} N-terminus is not essential for bi-directional coupling with RyR1. *Biochem. Biophys. Res. Commun.* 336:134–141.

Bannister, R.A., H.M. Colecraft, and K.G. Beam. 2008a. Rem inhibits skeletal muscle EC coupling by reducing the number of functional L-type Ca2+ channels. *Biophys. J.* 94:2631–2638.

Bannister, R.A., M. Grabner, and K.G. Beam. 2008b. The α_{1S} III-IV loop influences 1,4-dihydropyridine receptor gating but is not directly involved in excitation-contraction coupling interactions with the type 1 ryanodine receptor. *J. Biol. Chem.* 283:23217–23223.

Beam, K.G., and C. Franzini-Armstrong. 1997. Functional and structural approaches to the study of excitation-contraction coupling. *Methods Cell Biol.* 52:283–306.

Beam, K.G., and P. Horowicz. 2004. Excitation-contraction coupling in skeletal muscle. *In* Myology: Basic and Clinical. A.G. Engel and C. Franzini-Armstrong, editors. Third edition. McGraw Hill, New York. 257–280.

Beurg, M., C.A. Ahern, P. Vallejo, M.W. Conklin, P.A. Powers, R.G. Gregg, and R. Coronado. 1999. Involvement of the carboxy-terminus region of the dihydropyridine receptor β_{1a} subunit in excitation-contraction coupling of skeletal muscle. *Biophys. J.* 77:2953–2967.

Block, B.A., T. Imagawa, K.P. Campbell, and C. Franzini-Armstrong. 1988. Structural evidence for direct interaction between the molecular components of the transverse tubule/sarcoplasmic reticulum junction in skeletal muscle. *J. Cell Biol.* 107:2587–2600.

Buck, E., I. Zimanyi, J.J. Abramson, and I.N. Pessah. 1992. Ryanodine stabilizes multiple conformational states of the skeletal muscle calcium release channel. *J. Biol. Chem.* 267:23560–23567.

Carbonneau, L., D. Bhattacharya, D.C. Sheridan, and R. Coronado. 2005. Multiple loops of the dihydropyridine receptor pore subunit are required for full-scale excitation-contraction coupling in skeletal muscle. *Biophys. J.* 89:243–255.

Cheng, W., X. Altafaj, M. Ronjat, and R. Coronado. 2005. Interaction between the dihydropyridine receptor Ca^{2+} channel β-subunit and ryanodine receptor type 1 strengthens excitation-contraction coupling. *Proc. Natl. Acad. Sci. USA.* 102:19225–19230.

Cui, Y., H.S. Tae, N.C. Norris, Y. Karunasekara, P. Pouliquin, P.G. Board, A.F. Dulhunty, and M.G. Casarotto. 2009. A dihydropyridine receptor α_{1S} loop region critical for skeletal muscle contraction is intrinsically unstructured and binds to a SPRY domain of the type 1 ryanodine receptor. *Int. J. Biochem. Cell Biol.* 41:677–686.

El-Hayek, R., and N. Ikemoto. 1998. Identification of the minimum essential region in the II-III loop of the dihydropyridine receptor α_1 subunit required for activation of skeletal muscle-type excitation-contraction coupling. *Biochemistry.* 37:7015–7020.

Flucher, B.E., N. Kasielke, and M. Grabner. 2000. The triad targeting signal of the skeletal muscle calcium channel is localized in the COOH terminus of the α_{1S} subunit. *J. Cell Biol.* 151:467–478.

Flucher, B.E., R.G. Weiss, and M. Grabner. 2002. Cooperation of two-domain Ca^{2+} channel fragments in triad targeting and restoration of excitation-contraction coupling in skeletal muscle. *Proc. Natl. Acad. Sci. USA.* 99:10167–10172.

Freise, D., B. Held, U. Wissenbach, A. Pfeifer, C. Trost, N. Himmerkus, U. Schweig, M. Freichel, M. Biel, F. Hofmann, et al. 2000. Absence of the γ subunit of the skeletal muscle dihydropyridine receptor increases L-type Ca^{2+} currents and alters channel inactivation properties. *J. Biol. Chem.* 275:14476–14481.

Gach, M.P., G. Cherednichenko, C.S. Haarmann, J.R. López, K.G. Beam, I.N. Pessah, C. Franzini-Armstrong, and P.D. Allen. 2008. $\alpha_2\delta$ dihydropyridine receptor subunit is a critical element for excitation-coupled calcium entry but not for formation of tetrads in skeletal myotubes. *Biophys. J.* 94:3023–3034.

García, J., and K.G. Beam. 1994. Measurement of calcium transients and slow calcium current in myotubes. *J. Gen. Physiol.* 103:107–123.

García, J., T. Tanabe, and K.G. Beam. 1994. Relationship of calcium transients to calcium currents and charge movements in myotubes expressing skeletal and cardiac dihydropyridine receptors. *J. Gen. Physiol.* 103:125–147.

García, M.C., E. Carrillo, J.M. Galindo, A. Hernández, J.A. Copello, M. Fill, and J.A. Sánchez. 2005. Short-term regulation of excitation-contraction coupling by the β_{1a} subunit in adult mouse skeletal muscle. *Biophys. J.* 89:3976–3984.

García, K., T. Nabhani, and J. García. 2008. The calcium channel α_2/δ_1 subunit is involved in extracellular signalling. *J. Physiol.* 586:727–738.

Grabner, M., R.T. Dirksen, and K.G. Beam. 1998. Tagging with green fluorescent protein reveals a distinct subcellular distribution of L-type and non-L-type Ca^{2+} channels expressed in dysgenic myotubes. *Proc. Natl. Acad. Sci. USA.* 95:1903–1908.

Grabner, M., R.T. Dirksen, N. Suda, and K.G. Beam. 1999. The II-III loop of the skeletal muscle dihydropyridine receptor is responsible for the bi-directional coupling with the ryanodine receptor. *J. Biol. Chem.* 274:21913–21919.

Kugler, G., M. Grabner, J. Platzer, J. Striessnig, and B.E. Flucher. 2004a. The monoclonal antibody mAB 1A binds to the excitation—contraction coupling domain in the II-III loop of the skeletal muscle calcium channel α_{1S} subunit. *Arch. Biochem. Biophys.* 427:91–100.

Kugler, G., R.G. Weiss, B.E. Flucher, and M. Grabner. 2004b. Structural requirements of the dihydropyridine receptor α_{1S} II-III loop for skeletal-type excitation-contraction coupling. *J. Biol. Chem.* 279:4721–4728.

Leong, P., and D.H. MacLennan. 1998a. A 37-amino acid sequence in the skeletal muscle ryanodine receptor interacts with the cytoplasmic loop between domains II and III in the skeletal muscle dihydropyridine receptor. *J. Biol. Chem.* 273:7791–7794.

Leong, P., and D.H. MacLennan. 1998b. The cytoplasmic loops between domains II and III and domains III and IV in the skeletal muscle dihydropyridine receptor bind to a contiguous site in the skeletal muscle ryanodine receptor. *J. Biol. Chem.* 273:29958–29964.

Lorenzon, N.M., and K.G. Beam. 2007. Accessibility of targeted DHPR sites to streptavidin and functional effects of binding on EC coupling. *J. Gen. Physiol.* 130:379–388.

Lorenzon, N.M., C.S. Haarmann, E.E. Norris, S. Papadopoulos, and K.G. Beam. 2004. Metabolic biotinylation as a probe of supramolecular structure of the triad junction in skeletal muscle. *J. Biol. Chem.* 279:44057–44064.

Nakai, J., R.T. Dirksen, H.T. Nguyen, I.N. Pessah, K.G. Beam, and P.D. Allen. 1996. Enhanced dihydropyridine receptor channel activity in the presence of ryanodine receptor. *Nature.* 380:72–75.

Nakai, J., N. Sekiguchi, T.A. Rando, P.D. Allen, and K.G. Beam. 1998a. Two regions of the ryanodine receptor involved in coupling with L-type Ca^{2+} channels. *J. Biol. Chem.* 273:13403–13406.

Nakai, J., T. Tanabe, T. Konno, B.A. Adams, and K.G. Beam. 1998b. Localization in the II-III loop of the dihydropyridine receptor of a sequence critical for excitation-contraction coupling. *J. Biol. Chem.* 273:24983–24986.

Obermair, G.J., G. Kugler, S. Baumgartner, P. Tuluc, M. Grabner, and B.E. Flucher. 2005. The Ca^{2+} channel $\alpha_2\delta$-$_1$ subunit determines Ca^{2+} current kinetics in skeletal muscle but not targeting of α_{1S} or excitation-contraction coupling. *J. Biol. Chem.* 280:2229–2237.

Obermair, G.J., P. Tuluc, and B.E. Flucher. 2008. Auxiliary Ca^{2+} channel subunits: lessons learned from muscle. *Curr. Opin. Pharmacol.* 8:311–318.

Paolini, C., J.D. Fessenden, I.N. Pessah, and C. Franzini-Armstrong. 2004. Evidence for conformational coupling between two calcium channels. *Proc. Natl. Acad. Sci. USA.* 101:12748–12752.

Papadopoulos, S., V. Leuranguer, R.A. Bannister, and K.G. Beam. 2004. Mapping sites of potential proximity between the dihydropyridine receptor and RyR1 in muscle using a cyan fluorescent protein-yellow fluorescent protein tandem as a fluorescence resonance energy transfer probe. *J. Biol. Chem.* 279:44046–44056.

Proenza, C., C. Wilkens, N.M. Lorenzon, and K.G. Beam. 2000a. A carboxyl-terminal region important for the expression and targeting of the skeletal muscle dihydropyridine receptor. *J. Biol. Chem.* 275:23169–23174.

Proenza, C., C.M. Wilkens, and K.G. Beam. 2000b. Excitation-contraction coupling is not affected by scrambled sequence in residues 681-690 of the dihydropyridine receptor II-III loop. *J. Biol. Chem.* 275:29935–29937.

Proenza, C., J.J. O'Brien, J. Nakai, S. Mukharjee, P.D. Allen, and K.G. Beam. 2002. Identification of a region of RyR1 that participates in allosteric coupling with the α_{1S} ($Ca_V1.1$) II-III loop. *J. Biol. Chem.* 277:6530–6535.

Protasi, F., C. Franzini-Armstrong, and P.D. Allen. 1998. Role of ryanodine receptors in the assembly of calcium release units in skeletal muscle. *J. Cell Biol.* 140:831–842.

Protasi, F., H. Takekura, Y. Wang, S.R.W. Chen, G. Meissner, P.D. Allen, and C. Franzini-Armstrong. 2000. RYR1 and RYR3 have different roles in the assembly of calcium release units of skeletal muscle. *Biophys. J.* 79:2494–2508.

Protasi, F., C. Paolini, J. Nakai, K.G. Beam, C. Franzini-Armstrong, and P.D. Allen. 2002. Multiple regions of RyR1 mediate functional and structural interactions with α_{1S}-dihydropyridine receptors in skeletal muscle. *Biophys. J.* 83:3230–3244.

Schredelseker, J., V. Di Biase, G.J. Obermair, E.T. Felder, B.E. Flucher, C. Franzini-Armstrong, and M. Grabner. 2005. The β_{1a} subunit is essential for the assembly of dihydropyridine-receptor arrays in skeletal muscle. *Proc. Natl. Acad. Sci. USA.* 102:17219–17224.

Schredelseker, J., A. Dayal, T. Schwerte, C. Franzini-Armstrong, and M. Grabner. 2009. Proper restoration of excitation-contraction coupling in the dihydropyridine receptor β_1-null zebrafish *relaxed* is an exclusive function of the β_{1a} subunit. *J. Biol. Chem.* 284:1242–1251.

Sencer, S., R.V. Papineni, D.B. Halling, P. Pate, J. Krol, J.Z. Zhang, and S.L. Hamilton. 2001. Coupling of RYR1 and L-type calcium channels via calmodulin binding domains. *J. Biol. Chem.* 276:38237–38241.

Sheridan, D.C., L. Carbonneau, C.A. Ahern, P. Nataraj, and R. Coronado. 2003a. Ca^{2+}-dependent excitation-contraction coupling triggered by the heterologous cardiac/brain DHPR β_{2a}-subunit in skeletal myotubes. *Biophys. J.* 85:3739–3757.

Sheridan, D.C., W. Cheng, C.A. Ahern, L. Mortenson, D. Alsammarae, P. Vallejo, and R. Coronado. 2003b. Truncation of the carboxyl terminus of the dihydropyridine receptor β_{1a} subunit promotes Ca^{2+} dependent excitation-contraction coupling in skeletal myotubes. *Biophys. J.* 84:220–237.

Sheridan, D.C., W. Cheng, L. Carbonneau, C.A. Ahern, and R. Coronado. 2004. Involvement of a heptad repeat in the carboxyl terminus of the dihydropyridine receptor β_{1a} subunit in the mechanism of excitation-contraction coupling in skeletal muscle. *Biophys. J.* 87:929–942.

Sheridan, D.C., H. Takekura, C. Franzini-Armstrong, K.G. Beam, P.D. Allen, and C.F. Perez. 2006. Bidirectional signaling between calcium channels of skeletal muscle requires multiple direct and indirect interactions. *Proc. Natl. Acad. Sci. USA.* 103:19760–19765.

Slavik, K.J., J.-P. Wang, B. Aghdasi, J.-Z. Zhang, F. Mandel, N. Malouf, and S.L. Hamilton. 1997. A carboxy-terminal peptide of the

α_1-subunit of the dihydropyridine receptor inhibits Ca^{2+}-release channels. *Am. J. Physiol.* 272:C1475–C1481.

Tae, H.S., N.C. Norris, Y. Cui, Y. Karunasekara, P.G. Board, A.F. Dulhunty, and M.G. Casarotto. 2009. Molecular recognition of the disordered dihydropyridine receptor II-III loop by a conserved spry domain of the type 1 ryanodine receptor. *Clin. Exp. Pharmacol. Physiol.* 36:346–349.

Takekura, H., L. Bennett, T. Tanabe, K.G. Beam, and C. Franzini-Armstrong. 1994. Restoration of junctional tetrads in dysgenic myotubes by dihydropyridine receptor cDNA. *Biophys. J.* 67:793–803.

Takekura, H., C. Paolini, C. Franzini-Armstrong, G. Kugler, M. Grabner, and B.E. Flucher. 2004. Differential contribution of skeletal and cardiac II-III loop sequences to the assembly of dihydropyridine-receptor arrays in skeletal muscle. *Mol. Biol. Cell.* 15:5408–5419.

Tanabe, T., H. Takeshima, A. Mikami, V. Flockerzi, H. Takahashi, K. Kangawa, M. Kojima, H. Matsuo, T. Hirose, and S. Numa. 1987. Primary structure of the receptor for calcium channel blockers from skeletal muscle. *Nature.* 328:313–318.

Tanabe, T., K.G. Beam, J.A. Powell, and S. Numa. 1988. Restoration of excitation-contraction coupling and slow calcium current in dysgenic muscle by dihydropyridine receptor complementary DNA. *Nature.* 336:134–139.

Tanabe, T., K.G. Beam, B.A. Adams, T. Niidome, and S. Numa. 1990. Regions of the skeletal muscle dihydropyridine receptor critical for excitation-contraction coupling. *Nature.* 346:567–569.

Tuluc, P., N. Molenda, B. Schlick, G.J. Obermair, B.E. Flucher, and K. Jurkat-Rott. 2009. A $Ca_V1.1$ Ca^{2+} channel splice variant with high conductance and voltage-sensitivity alters EC coupling in developing skeletal muscle. *Biophys. J.* 96:35–44.

Ursu, D., S. Sebille, B. Dietze, D. Freise, V. Flockerzi, and W. Melzer. 2001. Excitation-contraction coupling in skeletal muscle of a mouse lacking the dihydropyridine receptor subunit γ_1. *J. Physiol.* 533:367–377.

Weiss, R.G., K.M.S. O'Connell, B.E. Flucher, P.D. Allen, M. Grabner, and R.T. Dirksen. 2004. Functional analysis of the R1086H malignant hyperthermia mutation in the DHPR reveals an unexpected influence of the III-IV loop on skeletal muscle EC coupling. *Am. J. Physiol. Cell Physiol.* 287:C1094–C1102.

Wilkens, C.M., and K.G. Beam. 2003. Insertion of α_{1S} II-III loop and C terminal sequences into α_{1H} fails to restore excitation-contraction coupling in dysgenic myotubes. *J. Muscle Res. Cell Motil.* 24:99–109.

Wilkens, C.M., N. Kasielke, B.E. Flucher, K.G. Beam, and M. Grabner. 2001. Excitation-contraction coupling is unaffected by drastic alteration of the sequence surrounding residues L720-L764 of the α_{1S} II-III loop. *Proc. Natl. Acad. Sci. USA.* 98:5892–5897.

Zimányi, I., E. Buck, J.J. Abramson, M.M. Mack, and I.N. Pessah. 1992. Ryanodine induces persistent inactivation of the Ca^{2+} release channel from skeletal muscle sarcoplasmic reticulum. *Mol. Pharmacol.* 42:1049–1057.